Die approbierte Originalversion dieser Diplom-/Masterarbeit ist an der Hauptbibliothek der Technischen Universität Wien aufgestellt (http://www.ub.tuwien.ac.at).

The approved original version of this diploma or master thesis is available at the main library of the Vienna University of Technology (http://www.ub.tuwien.ac.at/englweb/).

DIPLOMARBEIT

Implementation of Space-Time Codes in IEEE 802.11p-Based Systems

unter der Leitung von

Univ.Prof. Dipl.-Ing. Dr.techn. Christoph F. Mecklenbräuker
Dipl.-Ing. Veronika Shivaldova

Institute of Telecommunications
Technische Universität Wien

David Niklos

Kerschbaumgasse 2/1/11
1100 Wien

Matrikelnummmer: 0426436

Wien, im März 2012

Abstract

Vehicular communication networks promise to reduce the number and severity of traffic accidents, as well as to provide the capabilities for high data rate information and entertainment systems in vehicular environments. Numerous research activities have been carried out in the past years to develop communication facilities needed for establishing Intelligent Transportation Systems (ITS). This thesis first of all provides an overview of vehicular communications protocol specifications developed by IEEE (Institute of Electrical and Electronics Engineers). Performance and reliability of these specifications were investigated through MATLAB-based simulations. Past research activities have shown some deficiencies of the underlying communication standard IEEE 802.11p regarding transmission reliability. Vehicular communications opportunities provide a broad spectrum of safety-related applications. Especially for these issues, a high transmission reliability or robustness is essential. The transmission quality suffers from absence of continuous LOS (Line of Sight) wireless links between transmitter and receiver and time-variant channel conditions. In order to increase the transmission quality, the use of multi-antenna systems is suggested. This thesis provides an analysis of how the transmission reliability and performance can be increased by implementing MIMO (Multiple-Input Multiple-Output) transmission schemes. The utilization of multiple antennas at the transmitter requires the implementation of Space-Time Codes (STC). The investigated spatial coding schemes are Alamouti's space-time block code and the Golden Code. In the fourth chapter, this thesis provides an evaluation of the above mentioned MIMO schemes in comparison with the pure IEEE 802.11p SISO (Single-Input Single-Output) communication standard. This comparison is performed with various wireless radio propagation channel models suitable for vehicular communications.

Zusammenfassung

Um die Sicherheit und Effizienz des heutigen Straßenverkehrs zu steigern, werden Funkverbindungen zwischen benachbarten Fahrzeugen und Access-Terminals, sogenannten Road Side Units, geschaffen. Dieses Kommunikationsnetzwerk erschafft die Infrastruktur um diverse Dienste zu ermöglichen. Hauptaugenmerk ist das Angebot von sicherheitstechnischen Diensten, welche die Verkehrssicherheit erhöhen. Solche Dienste betreffen unter anderem die Meldung von Unfällen, gefährlichen Straßenbedingung oder Staus. Andere hauptsächlich kommerzielle Dienste wie z.B. High-Speed Internet Access im Fahrzeug werden einerseits das Fahrvergnügen steigern als auch die Finanzierung der nötigen Infrastruktur erleichtern.

Diese Diplomarbeit beschäftigt sich mit dem Kommunikationsprotokoll das diesem Netzwerk zugrundeliegt, IEEE 802.11p, und im Speziellen mit dem Physical Layer dieses Protokolls. Im Standard ist die Verwendung von einer Sendeantenne und einer Empfangsantenne definiert. Sicherheitsspezifische Nachrichten die mit einer hohen Sicherheit übertragen werden müssen haben einen hohen Stellenwert. Für den Fall, dass keine Sichtverbindung zwischen Sender und Empfänger auftritt, z.B. bei Abschattung durch ein weiteres Fahrzeug, verschlechtern sich die Bedingungen des Funkkanals beträchtlich. Die hohen Geschwindingkeiten der teilnehmenden Fahrzeuge erzeugen eine dopplerverschobene Mehrwegeausbreitung des Sendesignals, welches die Empfangsqualität zunehmend verschlechtert.

Um jener Verschlechterung entgegenzuwirken wird in dieser Diplomarbeit der Einsatz von Mehrantennensystemen, sowohl auf Seite des Senders als auch des Empfängers vorgeschlagen. Um dieses erweiterte Antennensystem bestmöglichst auszunutzen, werden sogenannte Space-Time Codes angewendet um die Übertragungssicherheit und Datenrate zu erhöhen. Anhand eines Software Simulators wird das Verhalten dieser erweiterten Technik analysiert. Durch die Simulation von verschiedenen virtuellen Funkkanälen, die für Fahrzeug spezifische Netzwerke designt wurden, kann eine realistische Evaluierung dieser Techniken erfolgen.

Acknowledgements

First of all, I want to give thanks to Professor Christoph Mecklenbräuker for providing me the opportunity to work on my diploma thesis in the exciting field of vehicular communications. His pleasant help and advice guided me in the right direction to finish this thesis.

I also want to give special thanks to Veronika Shivaldova for supervising me during my work in vehicular communications and for proofreading this thesis.

Furthermore, I would like to thank following people for informative discussions and advice on various topics concerning my diploma thesis: Arrate Alonso, Laura Bernadó, Georg Maier, Alexander Paier and Stefan Schwarz.

I'd also like to thank my parents Erna and Manfred, my aunt Roswitha and my brother Clemens for their patience and love as well as for providing me the possibilities to finish my studies in the fascinating field of electronics.

Finally, I am grateful to Christina Gradwohl, for her encouragement and support, but especially for lighting up my life.

Contents

1 Introduction 1

1.1 ITS Applications . . . 1
1.1.1 Traffic Safety-Related Applications . . . 2
1.1.2 Traffic Efficiency-Related Applications . . . 2
1.1.3 Value Added Services . . . 3
1.2 Introduction to IEEE 802.11p . . . 3
1.3 Radio Spectrum Allocation . . . 6
1.4 Overview of SISO-Simulator . . . 6
1.4.1 Concept . . . 7
1.4.2 Simulator Outputs . . . 10
1.5 Scope . . . 12

2 Systems with Multiple Antennas 13

2.1 MIMO Theory . . . 13
2.2 Overview of Space-Time Codes . . . 17
2.2.1 Space-Time Code Criteria . . . 17
2.2.2 Decoding . . . 19
2.2.3 Alamouti Space-Time Code . . . 19
2.2.4 The Golden Code . . . 23
2.2.5 Comparison . . . 25
2.3 Spatial Diversity in IEEE 802.11p-Based Systems . . . 25
2.3.1 IEEE 802.11n . . . 26
2.3.2 MIMO Channel Estimation . . . 27
2.3.3 Cyclic Delay Diversity . . . 29

3 MIMO-Simulator Description 32
3.1 Transmitter . . . 34
3.2 Radio Channel . . . 37
3.2.1 AWGN Channel Model . . . 39
3.2.2 Block-Fading Channel Model . . . 40
3.2.3 Jakes Spectrum Time-Variant Fading Model . . . 42
3.2.4 Geometry-Based Stochastic Channel Model . . . 43
3.2.5 Channel Normalization . . . 45
3.3 Receiver . . . 47
3.3.1 Eb/N0 Definition . . . 49
3.3.2 Simulator Output . . . 50

4 Simulation Results 52
4.1 AWGN Channel . . . 52
4.2 Block-Fading Channel . . . 56
4.3 Jakes Spectrum Channel Model . . . 60
4.4 Geometry-Based Stochastic Channel Model . . . 62

5 Conclusions 67

List of Acronyms 69

Bibliography 72

1

Introduction

Vehicular communications have gained much attention in research and standardization activities in the last years. In literature the abbreviations Vehicle-to-Vehicle (V2V) and Vehicle-to-Infrastructure (V2I) are often used to refer to this topic[1]. The main idea behind the vehicular communications is to establish a wireless link between nearby vehicles and access points, which will provide a real time communication network not only for drivers' information and advice, but also for higher level traffic management systems. Wireless vehicular communication networks are becoming more an more realistic, since research activities are constantly progressing. In this thesis possible extensions of the underlying standard called Wireless Access in Vehicular Environments (WAVE) will be considered and the increase of the communication reliability and throughput based on the simulation results will be presented.

1.1 ITS Applications

Various applications and services are defined for Intelligent Transport Systems (ITS). This section will list and describe some of them [1]. The main fields of applications for vehicular networks are:

- Traffic safety
- Traffic efficiency
- Value-added services

[1]The abbreviation V2X is used when referring to both V2V and V2I

1.1.1 Traffic Safety-Related Applications

The major goal of safety-related applications is Reducing the overall number and severity of traffic accidents. Safety-related applications messages have the highest priority in vehicular communication and inherit following functions:

- Emergency vehicle warning: This application informs the driver that an emergency vehicle is approaching and provides him with further information about how to avoid stalling the emergency vehicle.
- Overtaking vehicle warning: The overtaken driver gets the information that another vehicle intends to pass by, which actually secures the situation.
- Cooperative merging assistance: Drivers get advice about how the lane merging process could be carried out consensually.
- Post crash warning: Drivers receive these warnings if they approach a traffic accident. They get the information either by the crashed car itself or by a following car that detects a crashed vehicle warning and shares that message with other cars.
- Wrong way warning: Informs the driver about driving against the traffic and also warns close by vehicles about this dangerous traffic situation.

Other safety-related applications are warnings for hazardous road conditions, like slippery road or road works.

1.1.2 Traffic Efficiency-Related Applications

Vehicular communication networks will provide applications that deal with reducing the road traffic congestion and overall fuel consumption by providing necessary information to road operators or traffic management entities.

- Green light optimal speed information advises the driver about the correct speed to hit the next traffic light in the green phase.
- Route guidance: Information from traffic management systems can be used to obtain better route information and navigation.
- Variable traffic light phases: Durations of phases from traffic lights can be dynamically set to obtain better traffic flow.
- Speed limits information: Drivers get advice about permanent or temporary speed limits.

1.1.3 Value Added Services

To maintain a real time vehicular network, communication infrastructure like road side units[2] is needed. This deployment is quite costly. In order to finance these infrastructure commercial applications will be an appropriate extension. This will lead to an immense speedup in infrastructure deployment. The purpose of these applications is to generate benefits for costumers even when the density of infrastructure is low.

- Point of Interest Notification: Drivers will get information when they pass by regional places of interest. Additional information can be requested by the users.
- Parking Management: This service automatically charges parking fees and grants access to restricted areas.
- Local Advertising: Local offers of products and services can be forwarded to the driver by choice when passing-by a certain location.
- Internet Access: High speed Internet access can be granted to drivers and passengers for information and entertainment.
- Chasing Vehicles: Information about location as well as driving direction of stolen vehicles can be sent to relevant authorities.

Other issues like automated toll collection, SOS services and fleet management are just a few catchwords describing what vehicular connectivity stands for. The list of commercial applications is quite long and will soon get even longer when first commercial services pay off and more companies recognize these business opportunities.

1.2 Introduction to IEEE 802.11p

In order to establish the above mentioned applications and services, an entire communication architecture with several protocol families is required. The Institute of Electrical and Electronics Engineers (IEEE) Society provides communication standard specifications for wireless vehicular communication networks that are capable of the applications mentioned in Section 1.1. WAVE defines a complete layered protocol stack to address these applications entirely. The IEEE 802.11p [2] protocol provides specifications for the Physical (PHY) and Medium Access Control (MAC) layer which are the two lowest

[2] A Road Side Unit (RSU) is an access point in vehicular networks needed to distribute and maintain traffic relevant information.

layers of the vehicular communications architecture. This thesis predominantly deals with the physical layer characteristics.

The IEEE 802.11p protocol Physical Layer (PHY) defines the overall procedure of how information, i.e. payload data bits provided by higher layers, is prepared for the transmission over a wireless medium. The PHY layer is divided into two sublayers, the Physical Layer Convergence Protocol (PLCP) sublayer and the Physical Medium Dependent (PMD) sublayer. Dividing the PHY layer into two sublayers derives from the fact that the IEEE 802.11p protocol originates from the IEEE 802.11a protocol (Wi-Fi) that was adopted for vehicular communication requirements, which particularly implies longer Delay Spread Length (DSL) higher node mobility and strongly time-varying channels. In IEEE 802.11a the PMD sublayer defines all modulation and coding types, whereas the PLCP is defined for communication with the Medium Access Control (MAC) layer. The payload bits are contained in the PLCP Service Data Unit (PSDU) and are considered as the basis of all evaluation accomplished in this thesis.

IEEE 802.11p is an Orthogonal Frequency Division Multiplexing (OFDM) -based wireless communication protocol that utilizes in total 64 subcarriers. For data transmission only 48 subcarriers are used. Channel estimation can be accomplished bases on the 4 comb pilot subcarriers. The residual subcarriers are used as guard subcarriers[3] and are intendent for the compliance of certain radiation pattern for neighboring frequency bands. This radiation pattern are specified by radiation masks defined in the standard [3]. Data subcarriers are modulated by various modulation schemes, like Binary Phase Shift Keying (BPSK), Quadrature Phase Shift Keying (QPSK) and Quadrature Amplitude Modulation (QAM). Payload bits are encoded, using a convolutional encoder in conjunction with puncturing, to achive data rates from 3 to 27 Mbits/s. The bandwidth of IEEE 802.11p standard was doubled as compared to that of IEEE 802.11a,which results in doubling the sampling period. This modification result in doubling the overall duration of the guard interval were needed to better address the vehicular conditions and environment. Table 1.1 lists fundamental parameters of the IEEE 802.11p PHY layer.

In order to achieve desired data rates from 3 to 27 Mbit/s, eight different transmission regimes are specified [3]. Table 1.2 shows their characteristics. Various data rates can be obtained by combining different modulation schemes and coding rates. Three out of eight regimes are defined as compulsory. These are regimes 1, 3 and 5.

The encoded data bits are generally mapped to complex-valued symbols by modulation. The real and imaginary parts represent the in-phase and quadrature-phase

[3]Guard subcarriers are always set to zero to comply certain emission limits.

Bit rate (Mbits/s)	3, 4.5, 6, 9, 12, 18, 24, 27
Modulation mode	BPSK, QPSK, 16-QAM, 64-QAM
Code rate	1/2, 2/3, 3/4
Number of total subcarriers	64
Number of data subcarriers	48
Number of comb-pilot subcarriers	4
OFDM Symbol duration	8 μs
Cyclic prefix time (guard interval)	1.6 μs
FFT period	6.4 μs
Preamble duration (3 OFDM symbols)	32 μs
Channel bandwidth	10 MHz
Subcarrier spacing	0.15625 MHz
Sampling period	100 ns

Table 1.1: Physical layer parameters of IEEE 802.11p

Regime	Data rate (Mbits/s)	Modulation	Coding rate	Compulsory
1	3	BPSK	1/2	✓
2	4.5	BPSK	3/4	-
3	6	QPSK	1/2	✓
4	9	QPSK	3/4	-
5	12	16–QAM	1/2	✓
6	18	16–QAM	3/4	-
7	24	64–QAM	2/3	-
8	27	64–QAM	3/4	-

Table 1.2: Rate-dependent parameters

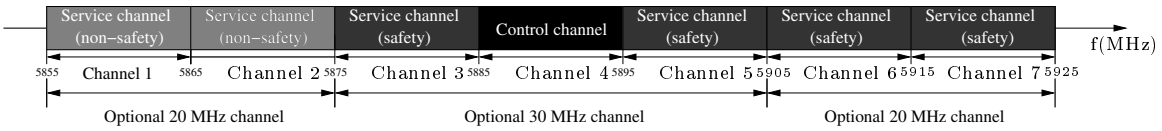

Figure 1.1: Frequency allocation for WAVE [4]

components of the associated subcarriers. Assembling these symbols in a so-called OFDM frame allows a more convenient view on processed data. Detailed information on how an OFDM signal in the discrete time domain is generated will be provided in Section 1.4.

1.3 Radio Spectrum Allocation

Wireless communications systems require allocated spectral bands to operate. These frequency bands must be reserved for the exclusive use of the desired system. Especially safety-related messages transmitted over an appropriate spectral band should not be affected by other wireless communication systems, neither by adjacent channels of the same system.

The Federal Communication Consortium has allocated a 75 MHz spectrum at 5850 – 5925 MHz in North America for vehicular communication issues. The European standardization consortia followed these recommendations and assigned the same frequency band for the use of ITS with the only constraint that the systems have to conform with certain prescribed radiation limits [4].

The 75 MHz spectral band is divided into seven 10 MHz channels appropriate for the appliance of IEEE 802.11p protocol as shown in Figure 1.1. One out of these seven channels is a control channel responsible for management information. Two channels are reserved for safety-related messages and the other five channels are so-called service channels. In order to obtain higher throughput the channels one and tow as well as the channels six and seven can be optionally combined to form a 20 MHz channel bandwidth. Furthermore the channels three, four and five (service and control channels) can be utilized as one dedicated channel to obtain higher data rates.

1.4 Overview of SISO-Simulator

Significant amount of preceding work has been carried out in the context of vehicular communications research. An important part of the research activities in this field is a

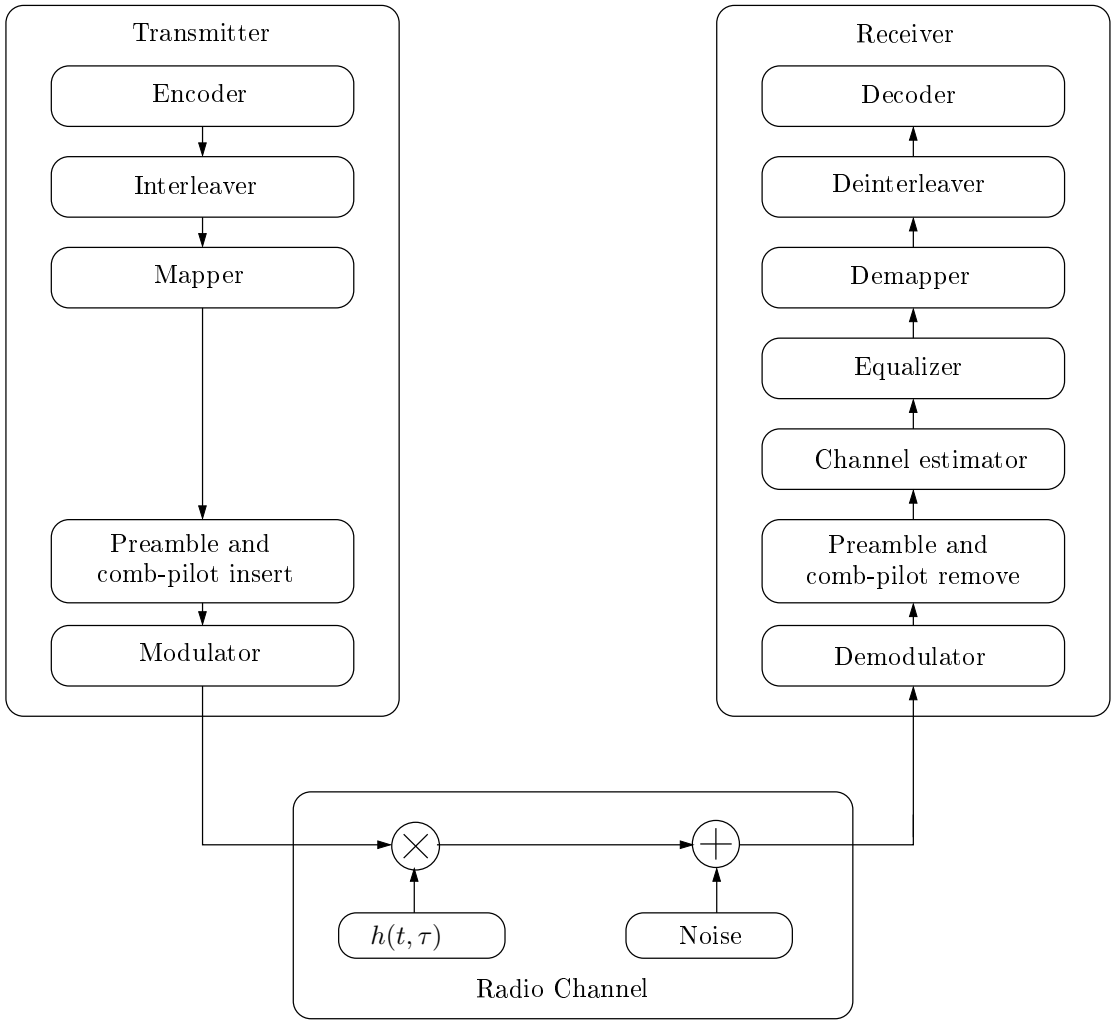

Figure 1.2: IEEE 802.11p PHY SISO Simulator Block Diagram

simulator-based research that reveals the transmission reliability of the PHY layer from IEEE 802.11p. Simulator output provides characteristic information of transmission reliability in terms of i.e. Bit Error Rate (BER) versus Eb/N0 curves. These curves illustrate numerical evaluations of PHY transmission capabilities. This section shows a brief introduction to the MATLAB-based simulator provided by the Forschungszentrum Telekommunikation Wien (FTW).

1.4.1 Concept

Figure 1.2 shows a block diagram of the WAVE simulator, that is conceptually divided into three key modules: the transmitter, the wireless radio propagation channel and the receiver, which are interconnected to a linear chain. Each module is further split up into several submodules. This section will give a conceptual view on how the trans-

mission chain is defined in the IEEE 802.11p standard. For detailed information on the individual steps refer to [3].

Transmitter

On the transmitter side of the simulator a data generator produces payload data bits randomly, with equally likely zeros and ones. This data bit stream represents the information to be transmitted provided. First, the data bits are processed by a convolutional encoder [3], which introduces redundancy used to combat the corruptive effect introduced by the wireless radio channel. The next step is interleaving, which is performed in order to map adjacent bits to non-adjacent OFDM subcarriers. This makes the link more robust against frequency-selective channel fading. Furthermore, the interleaved bits are mapped to the complex-valued symbols according to the modulation format from Table 1.2.

Assembling the symbols on the appropriate data subcarriers is the next stage, followed by the insertion of four comb pilot subcarriers. From this point on the data can be viewed in terms of OFDM symbols. A preamble interval is appended in front of the data containing a signal OFDM symbol and two so called long training OFDM symbols. IEEE 802.11p provides two types of pilot sequences, the comb pilot subcarriers and the two long training symbols. These sequences are predefined by the standard and are used to perform channel estimation, which is an appropriate approvimation of the generally complex-valued channel gains on each OFDM subcarrier. Figure 1.3 depicts the OFDM frame structure, which can be viewed on a time-frequency perspective. On the frequency axis the subcarriers are schematically drawn. The time axis shows the frame structure, starting with the preamble followed by OFDM data symbols. IEEE 802.11p defines ten short training sequences followed by two long training sequences, as shown in Figure 1.3. The short training sequences that do not appear on the figure are used for a coarse timing estimation. However they are not implemented in the simulator, because we assume perfect time synchronizatin. Time estimation performed at by the receiver by the correlator based on the short training sequence.

The symbol following after two long training sequences (block type pilots) is called signal field. It contains information about the actual transmission regime: modulation format, coding rate and frame length. This information is used by the receiver for decoding the whole OFDM frame. The signal field and the long training sequences are always BPSK modulated, regardless of which modulation format is used for the actual data. The coding rate used for encoding the signal field data is always 1/2. Combined with BPSK modulation it ensures the most reliable transmission quality within these

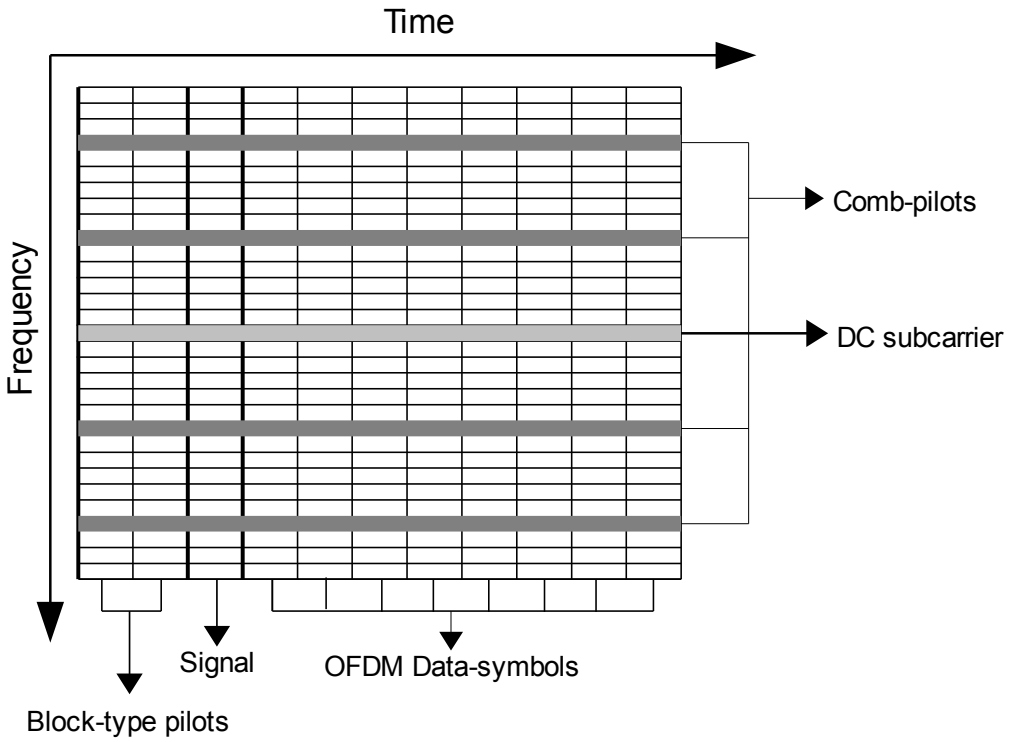

Figure 1.3: OFDM frame structure

specifications.

After the OFDM frame is completed, the modulation is performed, which is in fact an Inverse Fast Fourier Transformation (IFFT) operation. The complex-valued symbols on 64 subcarriers are converted into a 64 tap complex discrete time signal for each OFDM symbol. Compliant to an OFDM system the standard defines appending a cyclic prefix in front of the time discrete signal for every symbol, as shown in Figure 1.4. This cyclic prefix is also called guard interval (GI). It consists of the last 16 taps of the discrete time signal of the OFDM symbol copied and placed on the front. Thereby the discrete time domain signal is produced to fit the actual air interface. This signal represents the output of the transmit block shown in Figure 1.2.

Up to this stage an OFDM frame as shown in Figure 1.3 is converted into a time discrete signal with a structure according to Figure 1.4. The time domain signal starts with two times a training sequence for channel estimation, followed by the signal field and the remaining data OFDM symbols. The two long training sequences are grouped together, by using a double sized guard interval as shown in Figure 1.4.

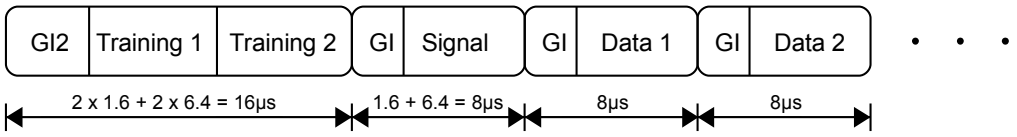

Figure 1.4: Time domain signal

Radio Channel

The transmitted signal undergoes channel distortion in a twofold manner. First, the discrete time signal is convolved with the channel impulse response. The characteristics of the wireless radio channel define the properties of the virtual simulated channel represented by the impulse response. Various channels, from simple static channels to more sophisticated time-variant channels, can be applied to the transmitted signal. Additionally an AWGN is added to the transmitted signal, which is already convolved with the channel impulse response. The actual power of the additive noise is predefined by the simulation Eb/N0 parameter.

Receiver

In the receive module the procedure is more or less the same as in the transmit module, just the other way around, starting with the demodulator which is in fact a Fast Fourier Transformation (FFT) operation. The OFDM demodulator output is again a frame that can be viewed on a time-frequncy grid perspective as presented in Figure 1.3. The next step is the removal of the preamble training symbols, the signal field and the comb type pilots. The training symbols together with the comb pilot subcarriers are used for channel estimation. The estimated channel coefficients are utilized by the equalizer to recover the transmitted data. Equalization is used to compensate for the effects of the physical channel. By that an estimate of the transmitted symbol stream is obtained. These symbols are demapped by the appropriate modulation type to obtain the encoded bit stream. The deinterleaver reverses both stages of interleaving performed in the transmitter. At the end, the resulting bit stream is decoded by a Viterbi-decoder to preserve the estimated payload data bits.

1.4.2 Simulator Outputs

The entire WAVE link level simulator provides an enormous amount of different settings for the transmitter and receiver, as well as channel models. In fact, the code allows in total 2304 different simulation settings. General input parameters are:

- Transmitter
  - Transmission regime
  - Frame length (bytes)
  - Bit energy to noise power spectral density ratio (E_b/N_0)
- Channel
  - AWGN
  - Block-fading
  - Time-variant
- Receiver
  - Channel estimator type
  - Equalizer type
  - Hard or soft demapper
  - Iterative decoding techniques

The simulation results are visualized on BER versus Eb/N0 curves. The uncoded BER and the decoded BER are shown together with the channel estimator's Mean Square Error (MSE). The BER is the error ratio obtained by comparing the payload data bits at the transmitter with the decoded bits at the output of the Viterbi-decoder at the receiver. The uncoded BER is the error ratio obtained by comparing the encoded bits at the output of the encoder with the undecoded bits at the input of the Viterbi-decoder. The MSE is the mean squared error calculated form the difference of the channel estimators channel coefficients and the true channel coefficients provided by the simulator.

Information obtained form these curves gives an advice of how to design the radio hardware in terms of transmit power, implemented transmit and receive techniques. They point out what specific setting may be best suited for vehicular communications, i.e. what kind of transmission regime, channel estimator, equalization type or decoding scheme is appropriate considering implementation issues like receiver complexity and hardware costs.

1.5 Scope

The receive signal level is varying over a large range due to of time variant multipath fading and blocked Line-of-Sight (LOS). These fading effects result in degradation of link reliability and cause packet losses. Retransmission initiated and controlled by MAC layer will cause significant time delays. Especially safety-related messages, as listed in section 1.1 obtain high significance, so the average number of retransmissions has to be as low as possible.

In this thesis we propose the use of multi antenna transmission and reception schemes (Multiple-Input Multiple-Output (MIMO)) to increase diversity and thus enhance the transmission quality. Utilization of Space-Time Coding (STC) will increase system diversity. Furthermore, these spatial encoding schemes may also increase the data rate by appropriate space-time coding.

Consequently the goal of this thesis is to evaluate advisable space-time block codes to increase link reliability and data rate. Applying various space-time codes requires a preliminary trade-off between increasing the data rate and diversity by choosing an appropriate code. Considering safety-related issues, the focus is on exploiting spatial diversity. With respect to the time varying nature of vehicular channels the emulated channel models should be as close to realistic as possible. This thesis evaluates the spatial diversity gain in vehicular communication environments, by that providing an advice on the benefits of applying space-time coding schemes to vehicular communications.

2

Systems with Multiple Antennas

2.1 MIMO Theory

Increasing the transmission quality or reducing the BER in a time variant multipath fading channel is an elaborate challenge. Concerning the pure Additive White Gaussian Noise (AWGN) channel, reducing the BER in an order 10 times could be done by increasing the Signal-to-Noise-Ratio (SNR) by a few dB only. Achieving the same BER reduction in a multipath channel is a more complex problem and may require higher SNR improvement. Previously, time and frequency diversity were frequently used as techniques for increasing transmission quality, but in recent years another type of diversity has been under investigation - spatial diversity.

This chapter deals with an introduction to wireless space-time coding and MIMO transmission schemes exploiting spatial diversity. The abbreviation MIMO refers to a wireless link with multiple antenna elements, utilized on both sides, the transmitter and the receiver. Similarly, the abbreviations Multiple-Input Single-Output (MISO) and Single-Input Multiple-Output (SIMO) are used when multiple antennas are employed only at the transmitter or the receiver, respectively. Multiple antenna systems have become a topic of significant interest for researchers during the last decade, as a technique promising increase throughput, reliability and transmission range. MIMO schemes have potential to address the main issues of wireless communications. Significant improvements that can be achieved are the following:

- Higher data rates

- Larger spectral efficiency
- More users per channel
- Improved coverage range
- Better interference suppression
- Higher reliability
- Less transmit power

Although multi-antenna schemes provide undeniable benefits, some of the drawbacks must be mentioned as well. Every additional antenna needs a full radio-frequency chain, including expensive radio frequency amplifiers and frequency converters for preparing the discrete time signal in order to suit radio transmission. Requirements for signal processing units are increased since multiple antenna transmission schemes require additional processing power, resulting in higher battery lifetime. Since every additional radio-frequency chain operates in the same bandwidth, each antenna interferes with the others [5] [6].

According to an overall description, Figure 2.1 shows a general block diagram of a typical MIMO communication system. The payload bit stream $b[m']$ is first processed by a Forward Error Correction Coding (FEC) and interleaving. The codebits $c[m'']$ are then mapped to higher level symbols $d[m''']$ with one of the defined modulation schemes. Afterwards the symbols are encoded into various symbols streams, one for each transmit antenna, depicted via the vector $\mathrm{x}[m]$. This procedure is called Space-Time Coding and will be explained in detail in Section 2.2.

As shown in Figure 2.1 the entire radio frequency part of the transmitter and receiver is included in the symbol-based baseband channel, according to Equation 2.1.

$$\mathrm{y}[m] = \mathrm{H}\ \mathrm{x}[m] + \mathrm{w}[m], \tag{2.1}$$

here the vectors $\mathrm{x}[m]$ and $\mathrm{y}[m]$ are the transmit and receive symbol vectors with the dimensions M_T and M_R respectively. Additive White Gaussian Noise is depicted by $\mathrm{w}[m]$. The channel matrix H in this model is assumed to stay constant during the transmission of $\mathrm{x}[m]$ and is further characterized in Equation 2.3.

$$\mathrm{H} = \begin{pmatrix} h_{1,1} & \dots & h_{1,M_T} \\ \vdots & & \vdots \\ h_{M_R,1} & \dots & h_{M_R,M_T} \end{pmatrix} \tag{2.2}$$

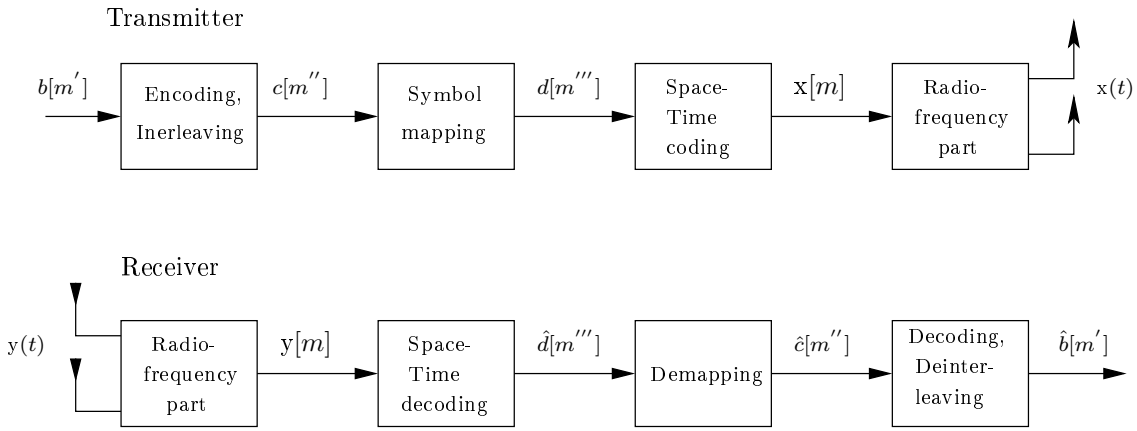

Figure 2.1: MIMO system model [5]

The coefficients $h_{i,j}$ depict the channel gains for each link referring to a distinct transmit and receive antenna pair. The size of the channel matrix is $M_R \times M_T$, with M_T as the number of transmit antennas and M_R as the number of receive antennas. At the receiver a space-time decoding is performed to obtain an estimated symbol stream $\hat{d}[m^{'''}]$. The space-time decoder is followed by demapping, decoding and deinterleaving, at end of which the received bitstream $\hat{b}[m^{'}]$ is obtained.

$$\mathrm{H} = \begin{pmatrix} h_{1,1} & \dots & h_{1,M_T} \\ \vdots & & \vdots \\ h_{M_R,1} & \dots & h_{M_R,M_T} \end{pmatrix} \tag{2.3}$$

The benefits achieved by multi-antenna transmission schemes can be represented in terms of MIMO gains. Various spatial codes are capable of exploiting these gains [5]:

- Array gain: It achieves an SNR improvement by coherently combining several signals of multiple transmit and receive antennas. To combine signals coherently channel knowledge is required. Utilizing array gain is also possible in SIMO and MISO systems with maximum ratio combining at the receiver or beamforming at the transmitter. The latter requires channel state information at the transmitter. Exploiting this gain shows up by a shift of the BER versus SNR curve.

- Diversity gain: Diversity at the transmitter is represented by multiple copies of the same signal transmitted in different time instants, over different frequencies or using different propagation paths. IEEE 802.11p already implements time and frequency diversity. Time diversity is introduced by the convolutional encoder and interleaver at the transmitter. Frequency diversity is introduced by spreading the bits over different OFDM subcarriers. The diversity grade can be further

increased by adding spatial diversity to the system. In systems with spatial diversity all the branches between the transmit and receive antennas experience independent fading effects, especially in Non-Line-of-Sight (NLOS) conditions. If one link fades, there is still enough information available on the other links. A rich scattering environment creates uncorrelated links. Diversity gain can be achieved without channel state information and its order is visualized by the slope of the BER versus SNR curve at high SNR values. Other types of diversity are code diversity and polarization diversity, which are out of the scope of this thesis.

- Coding gain: This gain can be achieved by applying FEC or STC, that result in both, diversity gain and coding gain.

- Multiplexing gain: The main reason for the research activities of MIMO systems is the so called multiplexing gain. It allows to increase the system capacity, i.e., the data rate, with no additional power consumption or bandwidth allocation. A general principle for increasing the data rate is the so-called spatial multiplexing scheme. Applying this scheme, M_T parallel data streams are transmitted by respective transmit antennas within the same channel. Every receive antenna obtains an superposition of various data stream. The receiver has to separate these data streams in order to recover the initially information.

- Beamforming gain: Beamforming is used to reduce interference from the other users in a communication system. Detailed channel state information is needed at the transmitter to apply beamforming. It creates a specific spatial signature of the transmit antenna array, but cannot be viewed as steering the entire antenna pattern of the transmit array.

The multiplexing gain and diversity gain are related to each other. Designing space-time codes always requires a tradeoff between those gains, in literature this is referred to the so called diversity-multiplexing tradeoff or frontier. The maximally achievable gains for diversity and multiplexing are bounded by the number of transmit and receive antennas as well as the channel characteristics. Codes that achieve the diversity multiplexing frontier are called perfect STC. Only codes with finite length can achieve full multiplexing gain and full diversity gain. Incremental SNR can be used to increase throughput or transmission reliability.

2.2 Overview of Space-Time Codes

Space-time coding characterizes how information is spread across various transmit antennas (space) and time (symbol periods). Spatial diversity gain can be exploited without Channel State Information (CSI) at the transmitter. The spatial information spreading should be well designed to achieve the diversity multiplexing frontier. Space-time codes are classified in Space-Time Block Codes (STBC) and Space-Time Trellis Codes (STTC). STBC are mostly used in conjunction with error correction codes. While when STTC is applied, the databits are directly mapped to the space-time encoded symbols and the error correction code is not needed. STTCs are an extension of the trellis codes to the case of multi-antenna transmit system and achieve better performance than STBC at the cost of a higher receiver complexity. As shown in Figure 2.1 the encoding is done on the symbol level instead of the bit level as in FEC. Generally speaking, a set of symbols is encoded in another set of symbols suitable for the transmission on spatially seperated streams. The encoded symbols $c_{i,j}$ represented by a codeword are summarized in form of a matrix X as shown in Equation 2.4. The index i defines the spatial stream, in other words, the number of the transmit antenna and the index j is related to the symbol interval. According to the utilization of an OFDM transmission system $c_{i,j}$ is placed in a per subcarrier manner in the j-th OFDM symbol on the i-th transmit antenna.

$$\mathrm{X} = \begin{pmatrix} c_{1,1} & c_{1,2} & \dots & c_{1,N} \\ c_{2,1} & c_{2,2} & \dots & c_{2,N} \\ \vdots & \vdots & \ddots & \vdots \\ c_{M_T,1} & c_{M_T,2} & \dots & c_{M_T,N} \end{pmatrix} \tag{2.4}$$

Applying Equation 2.4 to 2.1 and neglecting the time dependence of H results in 2.5. The size of the matrices Y, H and X are $M_R \times N$, $M_R \times M_T$ and $M_T \times N$, respectively. The number of symbol intervals occupied by one codeword is N (temporal code length). The channel is assumed to stay constant during the transmission of a space-time codeword [5].

$$\mathrm{Y} = \mathrm{H}\ \mathrm{X} + \mathrm{W} \tag{2.5}$$

2.2.1 Space-Time Code Criteria

Designing a Space-Time Code is a challenging task. This section provides a superficial presentation about key issues that affect the performance of Space-Time Codes, to give

the reader an idea about the important design criteria. To specify the performance of an STC, an expression for error probability is usually provided in literature. The Chernoff bound shown in Equation 2.6, provides an upper bound for the Pairwise Error Probability (PEP) of a Maximum Likelihood receiver to erroneously decide for the codeword X_2 when X_1 was transmitted. The term E_s/N_0 represents the signal to noise power ratio.

$$Pr\{\mathrm{X}_1 \to \mathrm{X}_2\} \leq \left(\prod_{i=1}^{r} \lambda_i\{B\}\right)^{-M_R} \left(\frac{E_S}{4N_0}\right)^{-rM_R} \tag{2.6}$$

This PEP is an average error probability over all channel realizations. This averaging process is a challenging task, therefore the Chernoff bound is a common clue to evaluate the error probability of various STC. The channel matrix H with the elements $h_{i,j}$ $\mathcal{CN}(0,1)$ being independent and identically distributed is assumed to stay constant during the transmission of one codeword. This refers to a so called Rayleigh fading MIMO channel model[1].

Equation 2.7 defines a so-called codeword difference matrix with two arbitrary codewords $X_1, X_2 \in \mathcal{C}$.

$$B = (\mathrm{X}_1 - \mathrm{X}_2)(\mathrm{X}_1 - \mathrm{X}_2)^H \tag{2.7}$$

r is the rank of B, and $\lambda_i\{\mathrm{B}\}$ are the nonzero eigenvalues. Since the pairwise error probability should be as low as possible, there are two design criteria for STC [5]:

- Rank criterion: In order to minimize the error probability the term $r\,M_R$ must be maximized. $r\,M_R$ defines the diversity gain and is represented by the slope of the error probability curve. Rank r is upper bounded by M_T, the number of transmit antennas. The rank criterion therefore states that B should have full rank. Achieving this with all pairs of the distinct codewords X_1 and X_2 the maximum diversity gain of $M_T\,M_R$ is obtained.

- Determinant criterion: The first factor in Equation 2.6 specifies the coding gain. Assuming that B has full rank, the determinant criterion states that the minimum determinant of B over all pairs of distinct codewords must be maximized. In other words, the product of all eigenvalues, which is the determinant of B, must be maximized. The coding gain refers to a horizontal shift of the BEP versus SNR curve.

[1] In most analytical considerations in literature a MIMO Rayleigh fading channel model is assumed.

2.2.2 Decoding

Several Decoding schemes are exploited for space-time codes. This section briefly describes the most important decoding schemes and their characteristics [5].

Maximum Likelihood Decoding

The Maximum Likelihood (ML) decision rule is shown in Equation 2.8 and refers to a maximization of the cost function $f(\mathrm{Y}|\mathrm{X})$. The detector chooses the transmit codeword matrix X, for which HX is closest to Y, in the sense of a minimum Euclidean distance. $\mathcal{C}$ defines the set of all possible codewords X. This decoding method results in optimum performance in terms of minimum codeword error probability and exploits all available diversity. The drawback is that the performance increase comes at the price of high complexity in case of large symbol alphabet size.

$$\hat{\mathrm{X}}_{ML} = arg \underset{\mathrm{X}\in\mathcal{C}}{max}\ f(\mathrm{Y}|\mathrm{X}) = arg \underset{\mathrm{X}\in\mathcal{C}}{min}\ ||\mathrm{Y}-\mathrm{HX}||^2 \tag{2.8}$$

Zero Forcing Decoding

The Zero-Forcing (ZF) decoding rule is shown in Equation 2.9 and is the result of a Least Square (LS) estimate of X. The big advantage is the low computational complexity with the drawback of noise enhancement. It eliminates the MIMO interference by applying the pseudoinverse of H. The nonlinear function $\mathcal{Q}(\cdot)$ denotes the quantization operation of a slicer, W is the noise component.

$$\hat{\mathrm{X}}_{ZF} = \mathcal{Q}\{(\mathrm{H}^H\mathrm{H})^{-1}\mathrm{H}^H\mathrm{Y}\} = \mathcal{Q}\{\mathrm{X} + (\mathrm{H}^H\mathrm{H})^{-1}\mathrm{H}^H\mathrm{W}\} \tag{2.9}$$

Minimum Mean Square Error Decoding

The Minimum Mean Squared Error (MMSE) approach combats the noise enhancement of the ZF solution and tries to reach a balance between noise enhancement and limiting MIMO-interference. The knowledge of the noise power level σ_w^2 is required for MMSE decoding.

$$\hat{\mathrm{X}}_{MMSE} = \mathcal{Q}\{(\mathrm{H}^H\mathrm{H} + \sigma_w^2\mathrm{I})^{-1}\mathrm{H}^H\mathrm{Y}\} \tag{2.10}$$

2.2.3 Alamouti Space-Time Code

In 1998 Siavash M. Alamouti introduced his STBC [6]. The proposed technique specifies a two-branch transmit diversity scheme and an arbitrary number of receive antennas.

Implementing this scheme with two transmit and one receive antenna provides the same diversity order as Maximum Ratio Receiver Combining (MRRC) with one transmit and two receive antennas. However, there is a 3 dB offset between MRRC 1×2 and Alamouti STBC 2×1 BER versus SNR curves, due to the fact that no channel state information is available at the transmitter. Alamouti's proposed technique is a simple transmit diversity scheme, that improves the quality of reception by low complexity processing on the transmitter. This scheme with two transmit antennas can easily be extended to an arbitrary amount of receive antennas to obtain a diversity order of $2M_R$[2]. This is done without any feedback from the transmit side, to interchange channel state information. This STBC needs only small computational complexity at both, the transmitter and the receiver and is accomplished with no bandwidth expansion.

Addressing the vehicular communication issues, MIMO schemes with two transmit antennas and one or two receive antennas are of special interest. Mounting more than two antennas on a vehicle is an implementation and financial issue, since the space for antenna installations on the car rooftop is limited and additional radio frequency chains are expensive. Therefore the Alamouti STBC 2×1 and 2×2 are considered in this thesis.

Encoding

Figure 2.2 illustrates how the Alamouti encoding procedure is performed and is valid for both the one and two receive antenna case. It defines how the modulated symbols are spread across two transmit antennas an two symbol time slots. In the first symbol period two symbols are simultaneously transmitted from both transmit antennas. The symbols x_1 and x_2 denote the first symbols from transmit antenna one and transmit antenna two respectively. During the subsequent symbol period, $-x_2^*$ is transmitted from antenna one and x_1^* from antenna two. As shown in Equation 2.11, two consecutive symbols are spatially encoded into four symbols. This encoding is done in space and time, however the encoding may also be done in space and frequency. Instead of two adjacent symbol periods, two adjacent subcarriers may be used (space-frequency coding). Note that the two different symbols x_1 and x_2 were transmitted in two symbol intervals. Hence, there is no change of the data rate at all. Equation 2.11 represents the codeword matrix of the scheme shown in Figure 2.2. One important fact of every Alamouti codeword matrix, is that X is always orthogonal ($\mathrm{X}^H\mathrm{X} = \mathrm{I}(|x_1|^2 + |x_2|^2)$), regardless of the underlying modulation scheme.

[2]Diversity order considerations are referred to mutually uncorrelated Rayleigh fading channel branches with perfect channel knowledge.

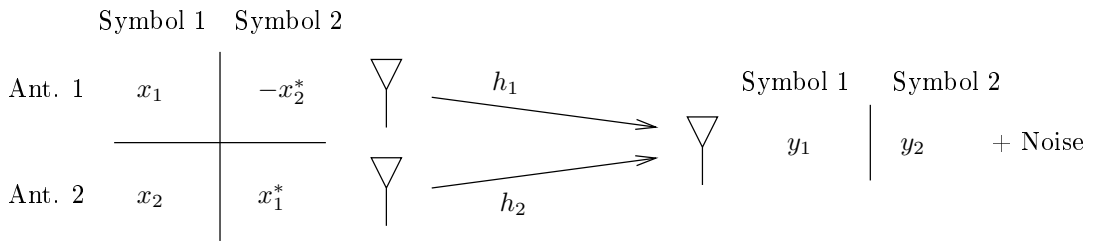

Figure 2.2: Alamouti 2×1

The difference matrix B in Equation 2.7 always achieves full rank, i.e., the Alamouti scheme obtains the maximum diversity order.

$$\mathrm{X} = \begin{pmatrix} x_1 & -x_2^* \\ x_2 & x_1^* \end{pmatrix} \tag{2.11}$$

Alamouti 2x1 Decoding

Figure 2.2 represents the transmission in the Alamouti-based MISO system in a symbol-based manner. A mathematical decoding description will be presented in this section. The receive symbols y_1 and y_2 are depicted in Equation 2.12, whith y_1 being the symbol received during the first symbol interval and y_2 during the second. The coefficients n_1 and n_2 denote the AWGN component. An important assumption regarding the channel gains is that they are assumed to stay constant during each group of two consecutive symbol intervals.

$$\begin{aligned} y_1 &= h_1 x_1 + h_2 x_2 + n_1 \\ y_2 &= -h_1 x_2^* + h_2 x_1^* + n_2 \end{aligned} \tag{2.12}$$

Rewriting the second line from Equation 2.12 by its conjugate complex yields to:

$$y_2^* = -h_1^* x_2 + h_2^* x_1 + n_2^* \tag{2.13}$$

Equations 2.12 and 2.13 rewritten in a matrix form are shown 2.14. The phase rotation of the noise component n_2 does not influence the effective SNR.

$$\begin{pmatrix} y_1 \\ y_2^* \end{pmatrix} = \begin{pmatrix} h_1 & h_2 \\ h_2^* & -h_1^* \end{pmatrix} \begin{pmatrix} x_1 \\ x_2 \end{pmatrix} + \begin{pmatrix} n_1 \\ n_2^* \end{pmatrix} = \tag{2.14}$$

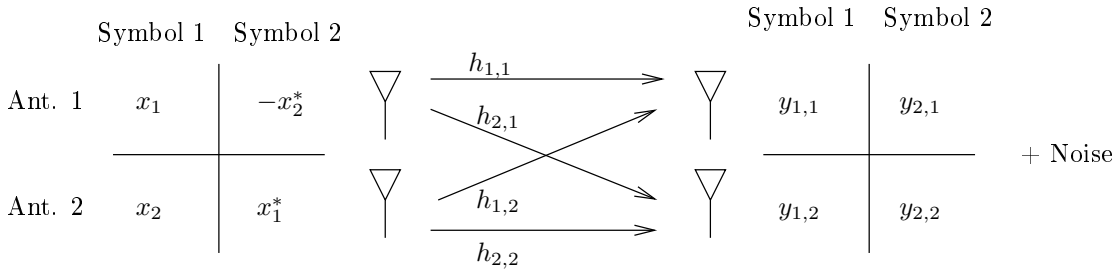

Figure 2.3: Alamouti 2×2

$$\widetilde{\mathrm{y}} = \widetilde{\mathrm{H}}\mathrm{x} + \widetilde{\mathrm{n}}$$

The virtual channel matrix $\widetilde{\mathrm{H}}$ is an orthogonal matrix with $\widetilde{\mathrm{H}}^H\widetilde{\mathrm{H}} = I(|h_1|^2 + |h_2|^2)$, i.e., its inverse is just its hermitian matrix. The pseudo inverse of $\widetilde{\mathrm{H}}$ shown in Equation 2.16 is required for compensation of the squared magnitude of the channel gains. This pseudoinverse $\overline{\mathrm{H}}$ can be viewed as an equalizer.

$$\overline{\mathrm{H}} = (\widetilde{\mathrm{H}}^H\widetilde{\mathrm{H}})^{-1}\widetilde{\mathrm{H}}^H \tag{2.15}$$

The ZF approach is shown in Equation 2.16.

$$\widehat{\mathrm{x}} = \overline{\mathrm{H}}\widetilde{\mathrm{y}} = \overline{\mathrm{H}}(\widetilde{\mathrm{H}}\mathrm{x} + \widetilde{\mathrm{n}}) = \mathrm{x} + \overline{\mathrm{H}}\widetilde{\mathrm{n}} \tag{2.16}$$

The decoded (equalized) symbols $\widehat{\mathrm{x}}$ are passed through a slicer. Optimal ML decoding can be achieved by applying a simple ZF decoder with minimum decoding complexity. This is accomplished by generating an orthogonal space-time encoding matrix as shown in Equation 2.11, resulting in an orthogonal virtual channel matrix (2.14) whos performance is nearly equal to that of Maximum Likelihood decoding. The Alamouti STBC is related to the group of orthogonal STBCs. The orthogonality of $\widetilde{\mathrm{H}}$ ensures that Maximum Likelihood decoding simplifies to a ZF decision [5].

Alamouti 2x2 Decoding

The Zero Forcing decoding scheme can easily be applied to the Alamouti 2×2 transmission scheme. The mathematical description of the decoding approach together with a schematic representation in Figure 2.3 will be presented in the following. The encoding procedure is the same as for Alamouti 2×1 and is shown in the spatial codeword matrix in Equation 2.11. Equation 2.17 and 2.18 show the signal received in the first and second symbol interval, respectively.

$$\begin{pmatrix} y_{1,1} \\ y_{1,2} \end{pmatrix} = \begin{pmatrix} h_{11} & h_{12} \\ h_{21} & h_{22} \end{pmatrix} \begin{pmatrix} x_1 \\ x_2 \end{pmatrix} + \begin{pmatrix} n_{1,1} \\ n_{1,2} \end{pmatrix} \tag{2.17}$$

$$\begin{pmatrix} y_{2,1} \\ y_{2,2} \end{pmatrix} = \begin{pmatrix} h_{11} & h_{12} \\ h_{21} & h_{22} \end{pmatrix} \begin{pmatrix} -x_2^* \\ x_1^* \end{pmatrix} + \begin{pmatrix} n_{2,1} \\ n_{2,2} \end{pmatrix} \tag{2.18}$$

The received symbols are denoted by $y_{i,j}$, with i representing the symbol period index, j the number of receive antennas and $n_{i,j}$ the AWGN component. The channel gains h_{jk} represent the fading conditions corresponding to the four MIMO links.

Rearranging Equations 2.17 and 2.18 in an appropriate manner, i.e., applying the conjugate complex to second lines of both equations, yields the Equation 2.19 with the virtual orthogonal channel matrix $\widetilde{\mathrm{H}}$.

$$\begin{pmatrix} y_{1,1} \\ y_{1,2} \\ y_{2,1}^* \\ y_{2,2}^* \end{pmatrix} = \begin{pmatrix} h_{11} & h_{12} \\ h_{21} & h_{22} \\ h_{12}^* & -h_{11}^* \\ h_{22}^* & h_{21}^* \end{pmatrix} \begin{pmatrix} x_1 \\ x_2 \end{pmatrix} + \begin{pmatrix} n_{1,1} \\ n_{1,2} \\ n_{2,1}^* \\ n_{2,2}^* \end{pmatrix} \tag{2.19}$$

$$\widetilde{\mathrm{y}} = \widetilde{\mathrm{H}}\mathrm{x} + \widetilde{\mathrm{n}}$$

Next steps of the decoding procedure are the same as in the Alamouti 2×1: generating the pseudo inverse of $\widetilde{\mathrm{H}}$ as in Equation 2.16, and applying the ZF equalization as shown in Equation 2.17. At the end the decoded symbols are sent through a slicer to obtain the estimated symbols with performance equal to that of an ML decoding. The encoding and decoding procedure has to be done for each pair of consecutive symbols x_1 and x_2.

2.2.4 The Golden Code

The Golden Code STBC is designed for MIMO systems with two transmit antennas, and it achieves full rate and full diversity. The code construction is based on the mathematical tool of cyclic division algebras, which yields a structured set of invertible matrices. The codewords can be considered as a subset of a cyclic division algebra. The authors of [7], [8] and [9] proposed the Golden Code independently of each other between 2003 and 2005. The name of the Golden Code initiates from the key role of the Golden number $\theta = \frac{1+\sqrt{5}}{2} = 1.618$ in the construction of this code. The codeword matrix X is generated as shown in Equation 2.20 [10]. Compared to Alamouti, the Golden Code transmission scheme provides twice the data rate, since four symbols are encoded into four code symbols, as shown in Equation 2.20.

$$X = \frac{1}{\sqrt{5}} \begin{pmatrix} \alpha[x_1 + x_2\theta] & \alpha[x_3 + x_4\theta] \\ i\sigma(\alpha)[x_3 + x_4\sigma(\theta)] & \sigma(\alpha)[x_1 + x_2\sigma(\theta)] \end{pmatrix} = \begin{pmatrix} c_{1,1} & c_{1,2} \\ c_{2,1} & c_{2,2} \end{pmatrix} \tag{2.20}$$

$$with \qquad i = \sqrt{-1} \qquad \theta = \frac{1+\sqrt{5}}{2} \qquad \sigma(\theta) = \frac{1-\sqrt{5}}{2} = 1 - \theta$$
$$\alpha = 1 + i - i\theta = 1 + i\sigma(\theta) \qquad \sigma(\alpha) = 1 + i - i\sigma(\theta) = 1 + i\theta$$

The Golden Code is optimal in several ways, as it achieves optimum STBC metrics:

1. Full-rate: Two symbols per channel use are transmitted.
2. Full-rank: The determinant of the difference of two arbitrary codewords is always different from zero. Therefore, the Golden Code achieves maximum diversity gain equal to $M_T M_R$.
3. Non-vanishing determinant: The minimum determinant ($\delta_{min} = \frac{1}{5}$) is independent of the constellation size (modulation alphabet).

Decoding

The Golden Code can be decoded with various schemes. The best performance is provided by ML decoding. Applying a ZF or an MMSE decoding scheme for the decoding of the Golden Code would result in poor performance, due to the non-orthogonality of this STBC. To achieve best decoding performance, a simple ML Brute Force (BF) or Sphere Decoder (SD) could be utilized. Equation 2.21 states the decision rule of an ML decoder.

$$\hat{\mathrm{X}}_{ML} = arg \min_{\mathrm{X} \in \mathcal{C}} ||\mathrm{Y} - \mathrm{HX}||^2 \tag{2.21}$$

The Golden Code 2×2 transmission scheme can be viewed as a system that maps a vector with four input symbols to a vector of four complex valued encoded output symbols. An ML Brute Force decoder will do an exhaustive search algorithm that considers each of the M^4 possible input matrices X in turn, computes the accordant channel output matrix HX and chooses the one, that is closest to the receive matrix Y in a minimum distance sense[3]. Thus the computational complexity of an ML BF decoder is proportional to M^4. This search algorithm requires adequate receiver processing

[3] M is the size of the modulation alphabet.

capability. Therefore an ML BF decoder for 16-QAM or 64-QAM modulation format is certainly not a practical approach. Complexity reduction for decoding the Golden Code has been intensively investigated in the last years. A ZF approach would end up in high BER, because of non-orthogonal space-time codewords. In [11] the authors provide a ML decoding scheme for the Golden Code that reduces the complexity from $\mathcal{O}(M^4)$ to $\mathcal{O}(M^{2.5})$ leading to a significant reduction of the receiver complexity.

2.2.5 Comparison

Table 2.1 provides a comparison of Space-Time Block Codes used in this thesis with respect to diversity gain d and multiplexing gain r. Codes that achieve the diversity-multiplexing frontier are called perfect STC. The Alamouti 2×1 and the Golden Code 2×2 are perfect codes, whereas the Golden Code doubles the data rate per utilized (OFDM-) symbol as compared to Alamouti STBC.

Space-Time Code	M_T	M_R	d	r	Data rate	Frontier attainment
Alamouti	2	1	2	1	ordinary	yes
Alamouti	2	2	4	1	ordinary	no
Golden Code	2	2	4	2	twice	yes

Table 2.1: Comparison of STBC

2.3 Spatial Diversity in IEEE 802.11p-Based Systems

Since IEEE 802.11p does not provide any structure for multi-antenna transmission schemes, some changes need to be introduced to the frame structure. MIMO channel estimation is not supported in IEEE 802.11p. In general, in order to estimate the 2×2 impulse responses obtained at the output of the four branch channel, four times the training data of SISO transmission is needed. A very promising candidate for an extended frame structure of the IEEE 802.11p protocol environment is the frame structure implemented in IEEE 802.11n, the MIMO wireless Local Area Network (LAN) protocol. The frame structure of the IEEE 802.11n standard seems to be the best suitable, due to the fact that both, the 802.11n and 802.11p originate from the 802.11a standard. This section provides detailed information of how the frame structure of IEEE 802.11n is used to suit for vehicular communication issues. A merging between 802.11p and 802.11n has to be accomplished to obtain MIMO transmission feasibility. Additionally, a mathematical description for MIMO channel estimation is provided in Section 2.3.2.

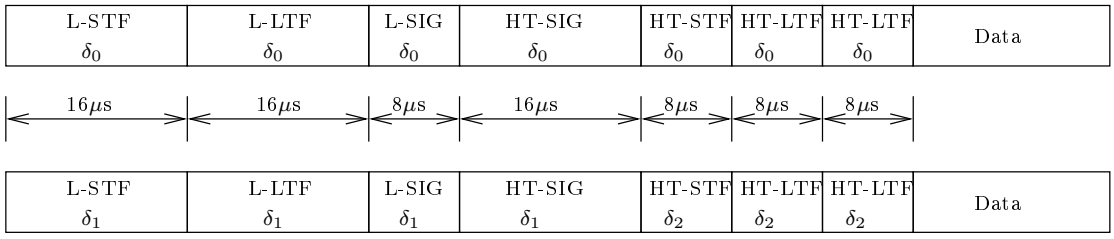

Figure 2.4: MIMO frame structure

2.3.1 IEEE 802.11n

IEEE 802.11n provides a variety of transmission regimes with up to 4×4 antenna transmission, optionally reduced guard interval and double bandwidth to obtain the highest data rate of 600 Mbits/s, which is achieved by using 4 spatial streams in a 40 MHz channel with a reduced 400 ns guard interval. In order to obtain compatibility with IEEE 802.11p SISO systems only the regimes compatible with IEEE 802.11p in terms of bandwidth, number of utilized data subcarriers and coding rate. Many functionalities in IEEE 802.11p and IEEE 802.11n are the same, since they have the same origin. Many software routines and hardware implementations are available for 802.11n. The main reason for using 802.11n is to obtain an higher reuse factor of these functionalities for further consideration in vehicular MIMO communications.

L-STF	Non-HT Short Training field	2 OFDM Symbols
L-LTF	Non-HT Long Training field	2 OFDM Symbols
L-SIG	Non-HT SIGNAL field	1 OFDM Symbol
HT-SIG	HT SIGNAL field	2 OFDM Symbols
HT-STF	HT Short Training field	1 OFDM Symbol
HT-LTF	HT Long Training field	1 OFDM Symbol

Table 2.2: Fields in MIMO frame structure [12]

Figure 2.4 shows the frame structure of IEEE 802.11n adopted to the specifications of 802.11p, i.e., the reduced bandwidth of 10 MHz and corresponding discrete time tap period of 100 ns. Every block in Figure 2.4 refers to one or two OFDM symbols, depending on the duration. Table 2.2 provides a list of abbreviations used in Figure 2.4. Therefore in the following, by 802.11n we refer not to the original 802.11n protocol structure, but rather to a fusion of 802.11p and 802.11n. The IEEE 802.11n standard defines two types of preamble, a mixed-mode preamble and a greenfield-mode preamble for higher data rates. In this thesis only the mixed-mode preamble will be considered, since this mode provides additional support of IEEE 802.11p SISO systems. Which is

strictly required for support of coexistence between SISO and MIMO vehicular communication systems.

The 802.11n 2×2 mixed-mode preamble starts with an 802.11p SISO preamble consisting of L-STF, L-LTF and L-SIG. The abbreviation L means low throughput or SISO. These three fields were already discussed in Section 1.4.1. The cyclically delayed copy of this preamble is transmitted form the second antenna. The cyclic delays used in this frame structure are depicted with $\delta_0 = 0\,\mu$s, $\delta_1 = -400\,\mu$s and $\delta_2 = -800\,\mu$s. Further explanation of the cyclic shift, called Cyclic Delay Diversity (CDD) will be given in Section 2.3.3. Despite the cyclic delay, the 802.11p SISO receivers are able to detect the signal from the second transmit antenna. 802.11p SISO receivers cannot decode 802.11n-based packets but retrieve the information from the SISO preamble that the channel is engaged during a certain time interval. The short training field (STF) is the same as for 802.11p but with a different cyclic delay at the second transmit antenna. The legacy or low throughput signal field (L-SIG) is followed by a high throughput signal field (H-SIG) that is spanned over two OFDM symbols. This new signal field contains information necessary for decoding the signal, like modulation and detection scheme, frame length, utilized STBC, GI length, CRC and channel sounding information. The HT-SIG field is followed by a short the training field, this HT-STF is used to retrain the AGC unit for a more precise estimation. The HT-STF is followed by two HT-LTF used for MIMO channel estimation. The second HT-LTF of the first transmit antenna is inverted to create an orthogonal space time pattern[4]. The two HT-LTF symbols are the same as one L-LTF symbol. Also the HT-STF is the same as the L-STF. The channel estimates are used to process the data part of the MIMO-OFDM signal. The comb pilot structure is different to 802.11p, since MIMO channel estimation requires a specific structure in pilot patterns [3] [12].

2.3.2 MIMO Channel Estimation

There are several approaches often used for MIMO channel estimation. The method presented in this section is referred in literature as time orthogonal method. The basic idea behind MIMO channel estimation, schematically shown in Figure 2.5. It refers to a system of equations with four linear independent equations and four unknown variables.

This section shows the basic estimation algorithm in an OFDM MIMO system like IEEE 802.11n. The transmitted and received preamble symbols, s and r are known at the receiver. The HT-LTF1 and HT-LTF2 symbols are BPSK modulated and in fact the same as the longtraining sequence in 802.11p. The HT-LTF sequence is shown in

[4]More information about this orthogonal pattern will be given in Section 2.3.2

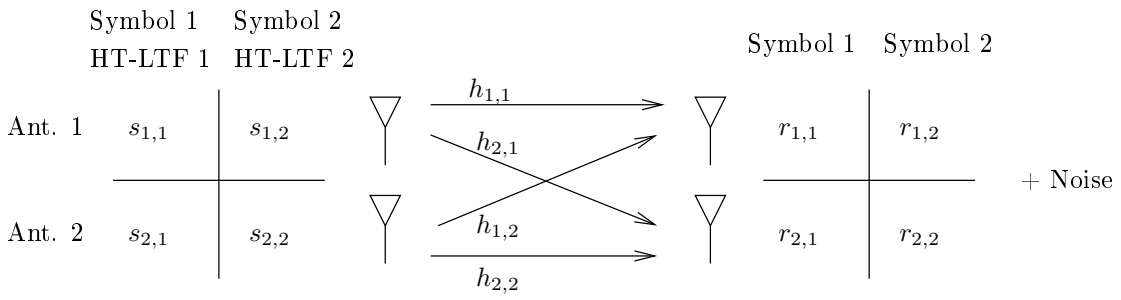

Figure 2.5: MIMO LS channel estimation

Equation 2.22 in the frequency domain. The guard subcarriers at the frequency band edges as well as the DC subcarrier are set at zero.

$$\begin{aligned} L \;=\; \{\, & 0,0,0,0,0,0,+1,+1,-1,-1,+1,+1,-1,+1,-1,+1,+1,+1,+1,+1,+1, \\ & -1,-1,+1,+1,-1,+1,-1,+1,+1,+1,+1,0,+1,-1,-1,+1,+1,-1,+1, \\ & -1,+1,-1,-1,-1,-1,-1,+1,+1,-1,-1,+1,-1,+1,-1,+1,+1,+1,+1, \\ & 0,0,0,0,0\,\} \end{aligned} \tag{2.22}$$

Pilot transmission (HT-LTF) viewed in a per subcarrier manner over two consecutive OFDM symbol intervals (HT-LTF1 and HT-LTF2) is shown in Equation 2.23. Here the channel matrix H is assumed to stay constant during the transmission of HT-LTF 1 and HT-LTF 2.

$$\mathrm{Y}_k = \mathrm{H}_k \mathrm{T}_k + \mathrm{W}_k \tag{2.23}$$

$$\begin{pmatrix} y^k_{1,1} & y^k_{1,2} \\ y^k_{2,1} & y^k_{2,2} \end{pmatrix} = \begin{pmatrix} h^k_{1,1} & h^k_{1,2} \\ h^k_{2,1} & h^k_{2,2} \end{pmatrix} \begin{pmatrix} t^k_{1,1} & t^k_{1,2} \\ t^k_{2,1} & t^k_{2,2} \end{pmatrix} + \begin{pmatrix} w^k_{1,1} & w^k_{1,2} \\ w^k_{2,1} & w^k_{2,2} \end{pmatrix}$$

Here $y^k_{i,l}$ is the receive signal, $h^k_{i,j}$ are the channel gains and $t^k_{j,l}$ the transmit signal. The indices i, j and l refer to the number of receive antenna, number of transmit antenna and OFDM symbol interval (HT-LTF1 and HT-LTF2), respectively. Due to BPSK modulation of HT-LTF and inverting the second HT-LTF on transmit antenna one, the matrix T_k is always $c\begin{pmatrix} 1 & -1 \\ 1 & 1 \end{pmatrix}$ with $c = 1$ or $c = -1$ (c depends on subcarrier index k). The inverse T_k^{-1} is the same as the pseudoinverse $\bar{\mathrm{T}}_k = (\mathrm{T}_k^H \mathrm{T}_k)\mathrm{T}_k^H$, computable with low complexity. Since T_k has always full rank the LS solution is not required. The channel estimation procedure is shown in Equation 2.24.

For the sake of completeness it is important to note that there exist other than this time-orthogonal methods, e.g. the time multiplexed MIMO channel estimation. In this methode the second HT-LTF from the first transmit antenna and the first HT-LTF form the second transmit antenna are set at zero. Thus, no transmission during these OFDM symbol intervals occurs, which is suboptimal for signal amplification issues (no constant envelope). The matrix T_k in this case is always $c\mathrm{I}$ (identity matrix), which leads to a more convenient approach for channel estimation.

$$\hat{\mathrm{H}}_k = \mathrm{Y}_k \mathrm{T}_k^{-1} = \mathrm{H}_k + \mathrm{W}_k \mathrm{T}_k^{-1} \tag{2.24}$$

The Equations 2.23 and 2.24 are valid for the case of 2×1 channel estimation, with the minor modifications regarding the size of the matrices Y_k and H_k (matrix size: 1×2).

2.3.3 Cyclic Delay Diversity

Applying the same signal on two transmit antennas will lead to unintended beamforming effects. To avoid such effects a technique called delay diversity can be implemented. With this technique the second discrete time signal is delayed by an arbitrary delay δ. This delay on a second transmit antenna sending the same signal as the first antenna will force the receiver to consider the signal from the second antenna as a delayed version of the signal from the first transmit antenna. The delayed replica of the same signal can be viewed as a multipath component. Therefore delay diversity will effectively increase the channel delay spread and may result in Inter Symbol Interference (ISI). This fact influences the choice of the antenna specific delay δ according to the conditions in Equation 2.25 [13].

$$\delta_{max} \leq N_G - N_{max}, \tag{2.25}$$

here N_{max} is the maximum delay of the radio propagation environment and N_G is the guard interval length. Therefore an extension of the delay diversity called CDD was developed to avoid delay constraints as depicted in Equation 2.25. Figure 2.6 shows a fundamental approach of how a cyclic delay is implemented in the transmission chain. Figure 2.7 shows an example of how a positive cyclic shift with $N_{FFT} = 8$, $\delta = 2$ and afterwards the cyclic prefix (guard interval) $N_{GI} = 3$ is applied to a discrete time signal.

As shown in Figure 2.6, the IEEE 802.11n standard define a cyclic shift (cyclic delay) to the transmit signal of the second antenna. The HT- and non-HT-portion (except HT-SIG) of the IEEE 802.11n preamble have shift values of $-400\,\mathrm{ns}$ (-4 taps) and $-800\,\mathrm{ns}$ (-8 taps), respectively. These cyclic shifts are applied in order to prevent unintentional

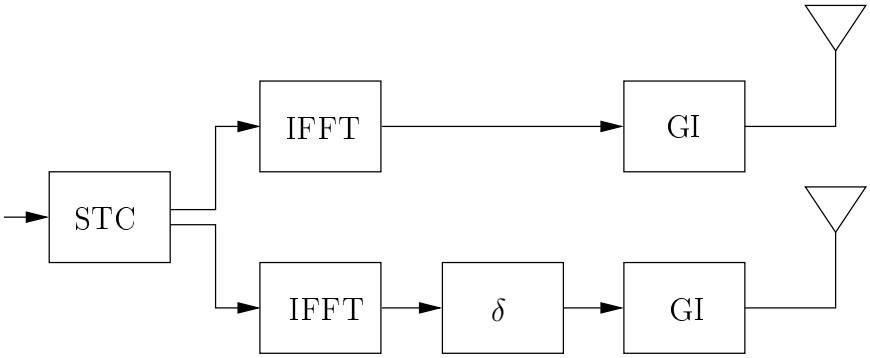

Figure 2.6: Block diagram of Cyclic Delay Diversity

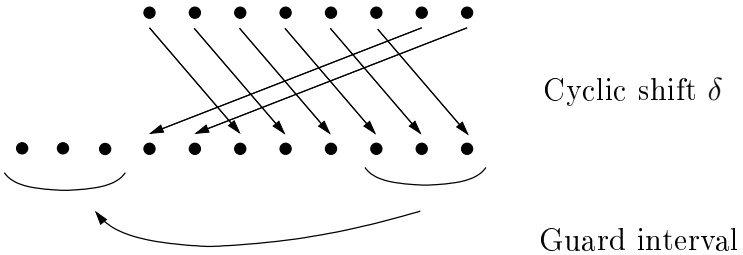

Figure 2.7: CDD and GI

beamforming effects that are unavoidable if similar signals are transmitted over different space-time streams. In fact, all fields shown in Figure 2.4 starting from L-STF up to HT-LTF define the same signal. Transmitting these signals over several spatial streams without a shift will result in undesired beamforming, especially in a low scattering environment. To do proper AGC the receive signal power level is estimated via the L-STF and H-STF. Short training fields (L-STF and HT-STF) needed for estimating the signal power for AGC must have low cross correlation. Therefore δ is set to 4 and 8 discrete time delay taps, because the STF autocorrelation is low at these delays [14]. Applying STC to the data part will end up in different spatial streams, so there is no need to apply a cyclic shift to the data part in general.

A receiver will observe modified channel conditions when CDD is utilized in the second transmit chain. The ability of using perfect CSI for decoding is provided by the simulator. Thus, no estimation process has to be accomplished. If there is a cyclic shift applied to the data part on the second transmit antenna, the utilized CSI has to be adopted as presented in Equation 2.26[5], with N_{FFT} is the number of FFT size[6]. A cyclic shift in the time domain shows up by a frequency dependent phase rotation for

[5] j in term e^{-jk} is the imaginary unit and not the transmit antenna index.
[6] IEEE 802.11p defines $N_{FFT} = 64$.

the channel coefficients.

$$h_{i,j} \rightarrow h_{i,j}\, e^{-jk\phi(j)}$$
$$\text{with} \quad \phi(j) = \frac{2\pi\,(j-1)\,\delta}{N_{FFT}} \tag{2.26}$$

Using the same cyclic shift for the training signal and for the data part, the channel estimator will consider the delayed signal as a channel effect and the equalizer will compensate it. Thus, the cyclic shift is viewed just as a part of the MIMO radio channel. Equation 2.26 depicts how channel state information changes if a cyclic shift δ is applied to the second transmit antenna and represented by a subcarrier k dependent phase shift. This fact is important when using perfect channel state information for decoding space-time codes.

3

MIMO-Simulator Description

This chapter will provide an overview of all three key modules of the MIMO vehicular communications simulator: the transmitter, the radio channel and the receiver. Figure 3.1 depicts these modules and shows in which way they are interconnected[1]. Applying multi antenna transmission and reception schemes changes the SISO simulator in various ways. Just the first few parts up to the mapper remain unchanged. Merging IEEE 802.11p and 802.11n protocol specifications results in a mixture of key properties of both protocols. The purpose of this chapter is to provide a detailed description of how this is accomplished.

[1] In Figure 3.1 a block diagram of a 2×2 simulator is provided. The differences to a 2×1 simulator are not depicted by a separate block diagram, but described in this chapter in detail.

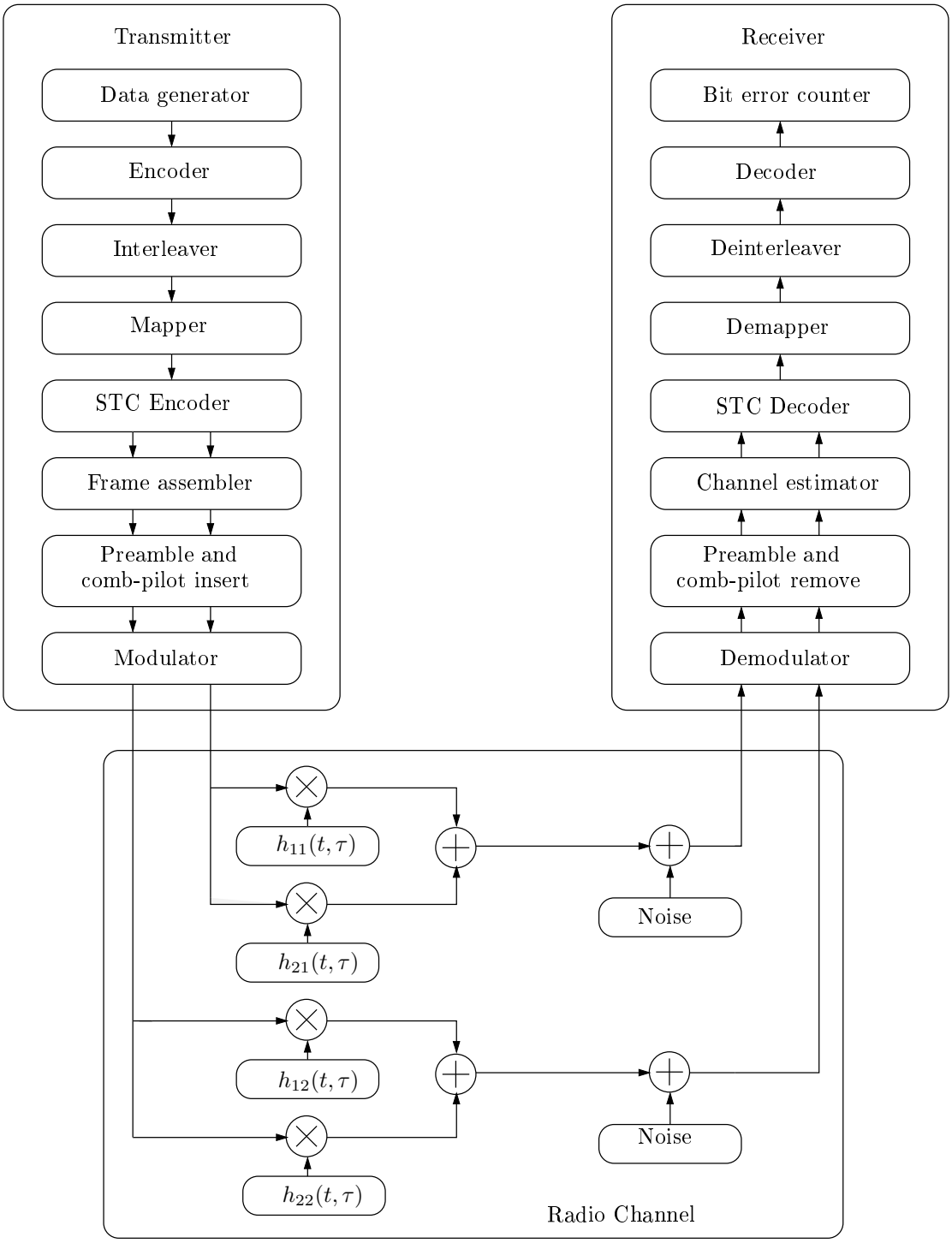

Figure 3.1: MIMO simulator modules

3.1 Transmitter

The very first block in the transmitter module is a data generator which is placed before the encoder. It randomly produces the payload data bits with equally likely zeros and ones, which are in practice initiated by higher layers. The generated amount of data which is needed for simulations is an input parameter to the simulator. The payload bit size together with the modulation and coding scheme determine the OFDM frame size.

The next block in the transmission chain following IEEE 802.11p specifications is the so called scrambler. A scrambling device is used to randomize the bit pattern, because often the payload bits from the MAC layer consist of long runs of zeros or ones due to tagging bits. This affects the whiteness property of the payload bit pattern. Furthermore scrambling helps to achieve a desired Peak-to-Average Power Ratio (PAPR). This device is usually implemented by shift registers and modulo 2 adders. The bit stream produced by the data generator is already random, so the scrambler is not needed for simulations and is therefore neglected.

One of the most important parts in telecommunications is FEC. The data passes through a convolutional encoder with a constraint length of 7, which introduces redundancy in the stream to combat corruptive channel influence (temporal diversity). This encoder utilizes a code rate of 1/2. Depending on the transmission regime, the code rate varies according to Table 1.2. Puncturing, which is accomplished by neglecting or deleting certain code bits periodically, is defined by vectors which are used to achieve the remaining code rates of 3/4 and 2/3, as defined by the protocol.

The encoded bits are directed to an interleaving stage, which is utilized to combat temporally long channel fades, which will result in burst errors. The term "long" in this context is related to a few sampling periods, which are several 100 ns. Interleaving is a predefined rearrangement of the bit stream, whith is reversed at the receiver node.

In order to obtain higher spectral efficiency the interleaved payload bits are mapped onto higher order modulation symbols. This step is carried out by the mapper, which chooses the modulation alphabet $\mathcal{A}$, depending on the defined transmission regime as depicted in Table 1.2. In order to achieve higher throughput, l consecutive bits are mapped onto a symbol $a[k] \in \mathcal{A} = \left\{a^{(1)}, a^{(2)}, \ldots a^{(M_a)}\right\}$ with $\mathcal{A}$ being an alphabet consisting of $M_a = 2^l$ different values. This results in a $l = ld(M_a)$ times higher throughput. Supported modulation alphabets for IEEE 802.11p are BPSK, QPSK, 16-QAM and 64-QAM. Considering this fact, the distance between consecutive points in the complex modulation plane will decrease with increasing modulation order. In order to achieve this throughput increase, the loss of reliability has to be taken into account,

due to transmit power constraints. Due to the use of Gray coded modulation schemes, in which the binary words corresponding to consecutive symbol points differ by only one bit, a symbol error will most likely result in only one bit error.

Up to the mapping part, the MIMO simulator is equal to the SISO simulator provided by FTW and follows IEEE 802.11p protocol specifications. Before the OFDM symbol assembler arranges the mapped symbols to the time frequency grid and adds the preamble, a space-time encoding process is accomplished. Figure 3.2 shows in a detailed way how the Alamouti and the Golden Code encoding together with the OFDM frame assembly are carried out in a per subcarrier manner. In order to recall the encoding procedure for both codes, Equation 3.1 (Alamouti) and Equation 3.2 state a mathematical description.

$$\mathrm{X} = \begin{pmatrix} x_1 & -x_2^* \\ x_2 & x_1^* \end{pmatrix} = \begin{pmatrix} c_{1,1} & c_{1,2} \\ c_{2,1} & c_{2,2} \end{pmatrix} \tag{3.1}$$

$$\mathrm{X} = \frac{1}{\sqrt{5}} \begin{pmatrix} \alpha[x_1 + x_2\theta] & \alpha[x_3 + x_4\theta] \\ i\sigma(\alpha)[x_3 + x_4\sigma(\theta)] & \sigma(\alpha)[x_1 + x_2\sigma(\theta)] \end{pmatrix} = \begin{pmatrix} c_{1,1} & c_{1,2} \\ c_{2,1} & c_{2,2} \end{pmatrix} \tag{3.2}$$

$$\text{with} \qquad i = \sqrt{-1} \qquad \theta = \frac{1+\sqrt{5}}{2} \qquad \sigma(\theta) = \frac{1-\sqrt{5}}{2} = 1 - \theta$$
$$\alpha = 1 + i - i\theta = 1 + i\sigma(\theta) \qquad \sigma(\alpha) = 1 + i - i\sigma(\theta) = 1 + i\theta$$

The Alamouti encoding process is described as follows (see Figure 3.2): The symbol stream $a[k] \in \mathcal{A}$ obtained from the mapper is grouped into blocks of two consecutive symbols. The elements of every block with index b are labeled x_1 and x_2. All these blocks are encoded by the Alamouti encoding procedure ending up in four code symbols $c_{i,l}^b$, which are x_1, x_2, $-x_2^*$ and x_1^* as described in Equation 3.1. The indices i and l refer to the transmit antenna number and the OFDM symbol number modulo 2, respectively.

Encoding the Golden Code is partly the same as in the Alamouti procedure. First, the symbol stream $a[k]$ is grouped into blocks of four consecutive symbols named x_1, x_2, x_3 and x_4. The encoding procedure is depicted in Equation 3.2 and ends up again in four encoded symbols $c_{i,l}^b$, which are labeled in the same way as in Alamouti encoding. It is noteworthy that using the Golden Code STBC, four symbols are encoded into four symbols. This is twice the number of origin symbols as in Alamouti and therefore the Golden Code offers double the data rate.

After encoding every block of consecutive symbols, the encoded symbols c are ar-

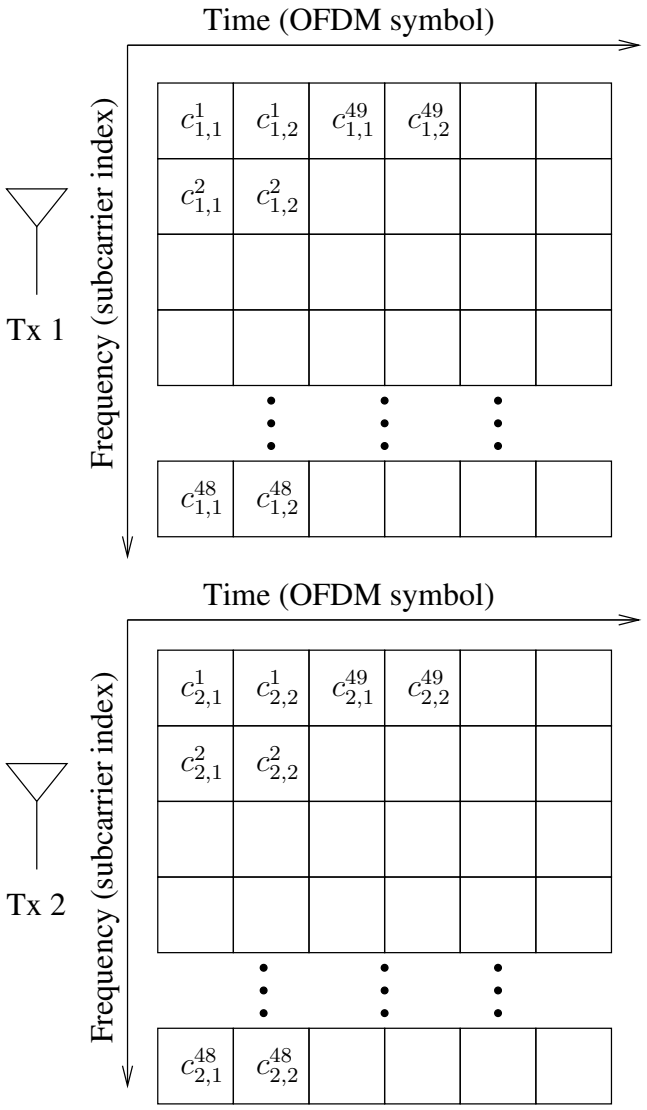

Figure 3.2: Space-time encoding

ranged at the various positions in the time-frequency grid, as shown in Figure 3.2.

After this encoding and arrangement procedure, the comb pilot subcarriers are inserted. IEEE 802.11n specifies a different comb pilot pattern than 802.11p, due to MIMO channel estimation. This pattern again represents an orthogonal space-time arrangement of pilot symbols like the long training sequence of the 802.11p preamble. After the data and pilot subcarriers are arranged in a time-frequency grid as shown in Figure 1.3, the 802.11n preamble is added (see Figure 2.4). For simulation related issues, only the HT-STF and two times the HT-LTF are implemented in the MATLAB code. The two HT-LTFs are utilized for MIMO channel estimation. In general the HT-STF symbols are used for fine timing information at the receiver. The simulator

does not need this field, since it is assumed to have perfect timing advice. However, the purpose of implementing this HT-STF in the simulator is to provide the ability to consider ISI in the implemented channel models. If the emulated channel is supposed to have larger delay spread than the guard interval, which may be the case in a real environment, ISI is unavoidable. This is considered in the simulator by implementing the HT-STF in front of the HT-LTFs. Due to the delay longer that the determined GI residual multipath components of HT-STF may appear in the HT-LTF OFDM signal, resulting in ISI. This affects the channel estimation procedure.

Necessary decoding information, such as frame length, code rate and modulation scheme used at the receiver is provided by the simulator itself and is not obtained from the HT-SIG field. This is an adequate approach since we compare different space-time coding schemes with SISO transmission. Afterwards, encoded and assembled data, provided in a time-frequency frame, is modulated by an IFFT transformation[2] with a mathematical description, shown in Equation 3.3.

$$s[n] = \frac{1}{\sqrt{K}} \sum_{k=0}^{K-1} S[k] e^{j2\pi \frac{kn}{K}} \tag{3.3}$$

According to IEEE 802.11n protocol specifications a cyclic shift of eight taps is applied to the discrete time signal of the second transmit antenna as shown in Figure 2.7, with $N_{FFT} = 64$ and $\delta = -8$ [3]. Subsequently, the guard interval of $N_{GI} = 16$ taps is added in front of every discrete time OFDM symbol.

3.2 Radio Channel

The wireless channel is the essential part of the simulator. The overall system performance is highly determined by the radio channel conditions. A typical radio channel consists of various signal paths from the transmitter to the receiver, specified as direct and indirect components. Due to the interaction between electromagnetic waves and the environment, the indirect components are referred to as reflected, scattered and diffracted signal paths. Representing realistic vehicular channel environments is a difficult task regarding processing power. Virtual channel models are created in order to emulate a wireless channel with appropriate computational needs. An extensive study

[2] IEEE 802.11p specifies a subcarrier rearrangement before IFFT: The subcarrieres 1 to 31 are mapped to IFFT inputs 1 to 31, whereas the subcarriers −32 to −1 belong to the IFFT inputs 32 to 63. The DC subcarrier remains unchanged.

[3] IEEE 802.11n defines a cyclic shift of −400 ns, this is equivalent to 8 taps since the sampling interval is 50 ns. IEEE 802.11p uses half the bandwidth of IEEE 802.11n, resulting in a double sampling interval of 100 ns. So the cyclic shift when merging 802.11n and 802.11p is set to −800 ns.

about vehicular channel characteristics is presented in [15]. This section provides a description of several vehicular MIMO channel models, which are used in the simulator and listed here by the increasing complexity: starting with a low complexity AWGN channel model and going through to a time variant Geometry-based Stochastic Channel Model (GSCM). Table 3.1 depicts an overview of implemented channels with respect to main channel properties. All channels are determined in the discrete time baseband model. In general, a discrete time impulse response $h_{i,j}[n,m]$ is defined by its delay m and discrete time dependence n.

Channel model	Noise	Multipath	Motion
AWGN	✓	-	-
Block-fading	✓	✓	-
Jakes spectrum	✓	✓	✓
GSCM	✓	✓	✓

Table 3.1: Channel model depiction

The input output relation of a 2×2 and 2×1 MIMO channel model is shown in Equations 3.4 and 3.5, respectively. The signals $s_i[n]$ and $r_j[n]$ refer to the transmit and receive signal, respectivly.

$$\begin{aligned} r_1[n] &= h_{1,1}[n,m] * s_1[n] + h_{1,2}[n,m] * s_2[n] + z_1[n] \\ r_2[n] &= h_{2,1}[n,m] * s_1[n] + h_{2,2}[n,m] * s_2[n] + z_2[n] \end{aligned} \tag{3.4}$$

$$r[n] = h_1[n,m] * s_1[n] + h_2[n,m] * s_2[n] + z[n] \tag{3.5}$$

Characteristic radio channel parameters are providing a deeper understanding of channel models and are shown in this section. A Power-Delay Profile (PDP) describes the temporal dispersiveness of a channel and provides key characteristics for entire protocol specifications. One of the most important parameters derived from the PDP is the Delay Spread (DS), which represents the temporal difference between the direct path and the last significant scattered path. The Root Mean Square Delay Spread (RMSDS) τ_{RMS}, which is given by the second centered moment of the PDP similarly specifies the temporal dispersiveness of a radio propagation channel. A temporal dispersive channel results in frequency selective fading. In Addition to frequency selectivity, a time dependence of the impulse response must be considered, since there is relative motion between the transmitter and the receiver ending up in Doppler shifted received

frequencies. This shift is determined by the relative velocity and characterized by f_D, which is named Doppler spread and indicates how the signal is spread over the frequency spectrum. In order to indicate the temporal and frequency selectivity, the parameters B_{coh} and T_{coh} are defined, which are the coherence bandwidth and the coherence time as depicted in Equation 3.6 and 3.7.

$$B_{coh} = \frac{1}{2\pi\tau_{RMS}} \tag{3.6}$$

$$T_{coh} = \frac{1}{2\pi f_D} \tag{3.7}$$

During the coherence time the channel remains approximately constant. The same statement holds for the coherence bandwidth that indicates a frequency interval in which the channel coefficients do not change. Results of a vehicular channel measurement campaign presented in [15], state the maximum values for $\tau_{RMS} = 400\,\text{ns}$ and $f_D = 1\,\text{kHz}$ for a highway scenario. This results in a coherence bandwidth of approximately 400 kHz and a coherence time of 0.16 ms. Due to IEEE 802.11p protocol specifications, the subcarrier spacing is 156.25 kHz and an ODFM symbol duration is $8\,\mu$s.

3.2.1 AWGN Channel Model

The electromagnetic field propagating through the wireless channel suffers from interference caused by other communication systems. Representing many different disturbing sources by a single random variable leads to a Gaussian distributed random variable, due to the central limit theorem. Equation 3.8 specifies the AWGN system model, in which H = I (identity matrix) wheras W represents the additive white Gaussian noise component. The model is presented in a per subcarrier manner, although the subcarrier index k is neglected. The discrete time impulse responses $h_{i,j}[n]$ for AWGN model 1 and 2 for 2×2 transmission, as well as the AWGN model for 2×1 transmission are depicted in Table 3.2. Since the impulse responses for every link branch remains constant during the entire signal transmission, the time dependence vanishes ($h_{i,j}[n,m] \rightarrow h_{i,j}[m]$).

$$\mathrm{Y} = \mathrm{H}\ \mathrm{X} + \mathrm{W} \tag{3.8}$$

The output sequence of the modulator, performing IFFT, is in general a complex valued sequence, therefore a complex valued AWGN component has to be added. The elements of W, which are $\{w_{i,l}\}$ are derived from the noise component $z[n]$ and added to the discrete time domain signal on every receive antenna (see Figure 3.1). The FFT at the receiver does not change the statistical properties of the noise component. Therefore

Impulse response	AWGN model 1 (2x2)	AWGN model 2 (2x2)	AWGN (2x1)
$h_{1,1}[n,m]$	$\delta[m]$	$\delta[m]$	$\delta[m]$
$h_{1,2}[n,m]$	0	$\delta[m]$	$\delta[m]$
$h_{2,1}[n,m]$	0	$\delta[m]$	-
$h_{2,2}[n,m]$	$\delta[m]$	$\delta[m]$	-

Table 3.2: AWGN impulse response (non-normalized)

both $z[n]$ and $w_{i,l}$ are complex valued, stationary, zero mean, circularly symmetric, Gaussian distributed random processes, with independent real and imaginary parts. Equation 3.9 provides the probability density function of $w_{i,l}$ with the noise variance σ_w^2. Since $w_{i,l}$ is zero mean, the variance is equal to the noise power. [4]

$$\begin{aligned} f_w(w) &= f_{w_R}(w_R) f_{w_I}(w_I) \\ &= \frac{1}{\sqrt{2\pi\sigma_w^2/2}} \exp(-\frac{1}{2}(\frac{w_R}{\sigma_w/\sqrt{2}})^2) \frac{1}{\sqrt{2\pi\sigma_w^2/2}} \exp(-\frac{1}{2}(\frac{w_I}{\sigma_w/\sqrt{2}})^2) \\ &= \frac{1}{\pi\sigma_w^2} \exp(-\frac{w_R^2 + w_I^2}{\sigma_w^2}) \\ &= \frac{1}{\pi\sigma_w^2} \exp(-\frac{|w|^2}{\sigma_w^2}), \end{aligned} \tag{3.9}$$

3.2.2 Block-Fading Channel Model

Multipath propagation environment causes the signal to occur at the receiver in multiple copies. Interfering electromagnetic waves result in frequency selective fading. The temporally first contribution path from transmitter to receiver is usually the strongest part with respect to signal power. Other receive signal portions form scattering environment arrive later at the receiver. Therefore, the propagation distance is longer compared to the first path, and the power of later arriving signal copies will be less. This behavior is addressed by a monotonically decaying PDP. The approach to implement the multipath fading channel in a simulator is to define a Rayleigh fading channel with exponential decaying PDP. This kind of PDP is often used to characterize multipath fading channels. With respect to IEEE 802.11p protocol specifications, the guard interval length is 16 taps (1.6 μs), therefore the channel DSL is set to 15 taps in order to obtain no ISI within this channel model. The DSL of 15 taps (1.5 μs) represents a propagation delay difference of 450 m between the direct path and the last considered scattered path. Equation 3.10 shows how the impulse response is computed from a mean PDP

with exponential decay, with an RMSDS $\sigma = 400\,\text{ns}$[4] and T_s as the sampling time. In order to obtain random channel realizations, every tap of the exponentially decaying PDP is multiplied with a Rayleigh distributed random variable. The reason of using the Rayleigh distributed random variables at this point is the following: the in-phase and quadrature-phase of the received signal are Gaussian distributed, the joint probability density function is a product of a uniformly distributed phase and a Rayleigh distributed magnitude [16]. Every 2×1 and 2×2 branch impulse response is computed in this way. This is a common NLOS radio propagation channel model [4].

$$h[m] = e^{-\frac{mT_s}{2\sigma}} \tag{3.10}$$

The block fading assumption states that the impulse response remains constant during the transmission of one OFDM frame ($h_{i,j}[n,m] \rightarrow h_{i,j}[m]$). This assumption is valid when the ODFM frame duration is smaller than the coherence time of the channel. Figure 3.3 provides a diagram of a typical impulse response magnitude $|h[l,m]|$ of a block fading channel. In OFDM systems it is assumed that the channel remains constant during the transmission of one OFDM symbol. Due to time invariant channel modeling, the channel remains constant during the whole frame duration[5].

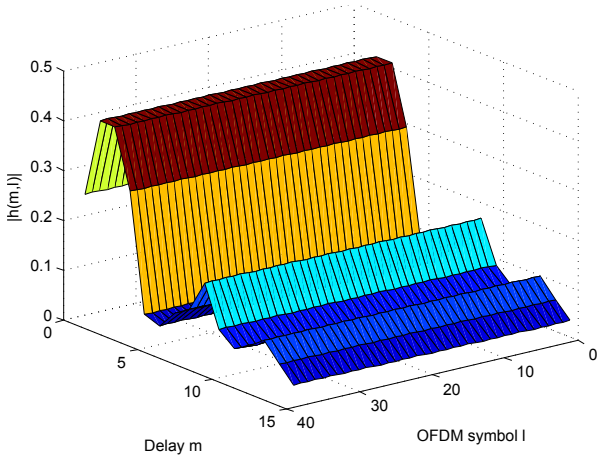

Figure 3.3: Block-fading channel

Kronecker Model

The impulse responses of the 2×2 links are generated as described in the previous section. This generation process assumes totally uncorrelated branches. However, in real scenarios this assumption may not always hold due to different reasons, such as

[4] 400 ns refer to measurement results in a highway scenario in [15] (worst case).
[5] In this example the frame consists of 39 OFDM symbols.

insufficient scattering environment or spacing between transmit or receive antennas. A common way to introduce correlations between MIMO link branches is the so-called Kronecker model represented in Equation 3.11, where the matrices R_{Tx} and R_{Rx} are positive definite Hermitian matrices representing the correlations on the transmitter and the receiver side, respectively [5]. H_w represents the uncorrelated channel matrix of size $N_R \times N_T$ in a per subcarrier manner.

$$\mathrm{H} = \sqrt{\mathrm{R}_{Rx}}\ \mathrm{H}_w\ \sqrt{\mathrm{R}_{Tx}}^{T} \tag{3.11}$$

Further information about the assembly of R_{Rx} and R_{Tx} is given in Equation 3.12[6]. The individual correlations between the transmit and receive antenna pair are represented by ρ_{Tx} and ρ_{Rx}, respectively.

$$\mathrm{R}_{Tx} = \begin{pmatrix} 1 & \rho_{Tx} \\ \rho_{Tx}^{*} & 1 \end{pmatrix}, \qquad \mathrm{R}_{Rx} = \begin{pmatrix} 1 & \rho_{Rx} \\ \rho_{Rx}^{*} & 1 \end{pmatrix} \tag{3.12}$$

These correlations are usually implemented in the frequency domain. In order to do so, Equation 3.11 is applied in a per-subcarrier manner to the channel coefficients represented by H_w. If the channel coefficients are available in the time domain, Equation 3.11 is applied to H_w representing the impulse responses in a per delay-tap manner.

3.2.3 Jakes Spectrum Time-Variant Fading Model

The assumption that a channel state remains constant during an entire OFDM frame duration is hardly realistic. In practice fluctuations of channel states during the transmission of a frame or even of an OFDM symbol are frequently obtained. Therefore, time variant channels must be considered in order to simulate more realistic channel conditions. The time variety of channel states originates from relative movements of transmitter, receiver and even scatterers. The mobility of those components result in Doppler shifted signals. These signals are derived from several scatterers, all with different Doppler shifted copies of the transmitted signal that add at the receiver.

Jakes spectrum time-variant fading channel model is introduced in [17] and further described in [4]. It considers an exponential decaying PDP introduced, in Section 3.2.2. The Doppler shift depends on the relative velocity of transmitter, receiver and scattering components. The entire model consists of both, a time selective and a frequency selective part of the impulse response. The latter one is determined by the exponen-

[6] In order to compute the root of a matrix R, the eigenvalue decomposition is used. With a matrix V including the eigenvectors and a diagonal matrix Λ including the eigenvalues of R. $\mathrm{R} = \mathrm{V}\Lambda^{\frac{1}{2}}\mathrm{V}^{-1}\mathrm{V}\Lambda^{\frac{1}{2}}\mathrm{V}^{-1}$, thus $\sqrt{\mathrm{R}} = \mathrm{V}\Lambda^{\frac{1}{2}}\mathrm{V}^{-1}$.

tially decaying PDP, whereas the time selective part is determined by the relative speed between transmitter and receiver, as well as by a predefined number of considered propagation paths. For every delay-tab of the exponentially decaying PDP, a fixed Doppler spectrum is applied. This model corresponds to a typical NLOS environment with a moving transmitter. In case of 2×1 and 2×2 MIMO channels, every link or branch $h_{i,j}[n, m]$ is modeled by uncorrelated impulse responses determined by this channel model. Figure 3.4 provides a diagram of a typical impulse response of Jakes spectrum channel model. Since NLOS scenarios are modeled, the channel changes quickly during one frame duration and even during one OFDM symbol.

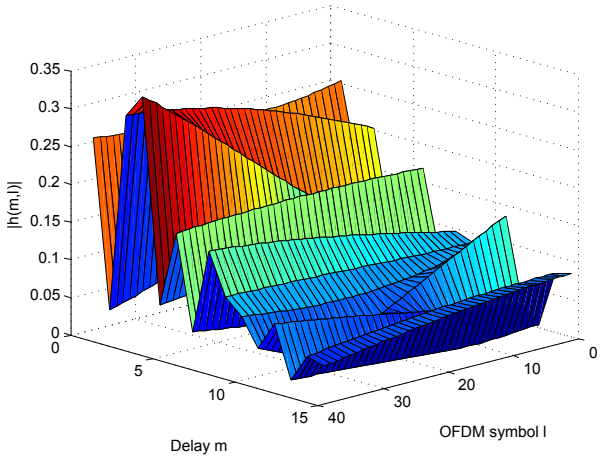

Figure 3.4: Jakes specturm fading channel

3.2.4 Geometry-Based Stochastic Channel Model

A ray-based stochastic approach to model radio propagation channels is carried out in a GSCM. This approach is designed for a highway scenario and considers four lanes (two in each direction), a moving transmitter, static receiver and static as well as moving scatterers. The basic idea of this model is that the geometry of the channel environment is randomly generated according to measured statistical parameters provided in [18]. Various vehicular channel measurement campaigns have been accomplished to determine key statistical properties such as LOS, deterministic and diffuse scattering components used in this model. In order to consider these components, a two-dimensional geometry is defined with different types of point scatterers, which are mobile discrete, static discrete and diffuse scatterers. These scatterers are placed in a two-dimensional plane according to a predefined statistical distribution (density) as presented in Figure 3.5. This approach predominantly considers V2I channels with a strong LOS component.

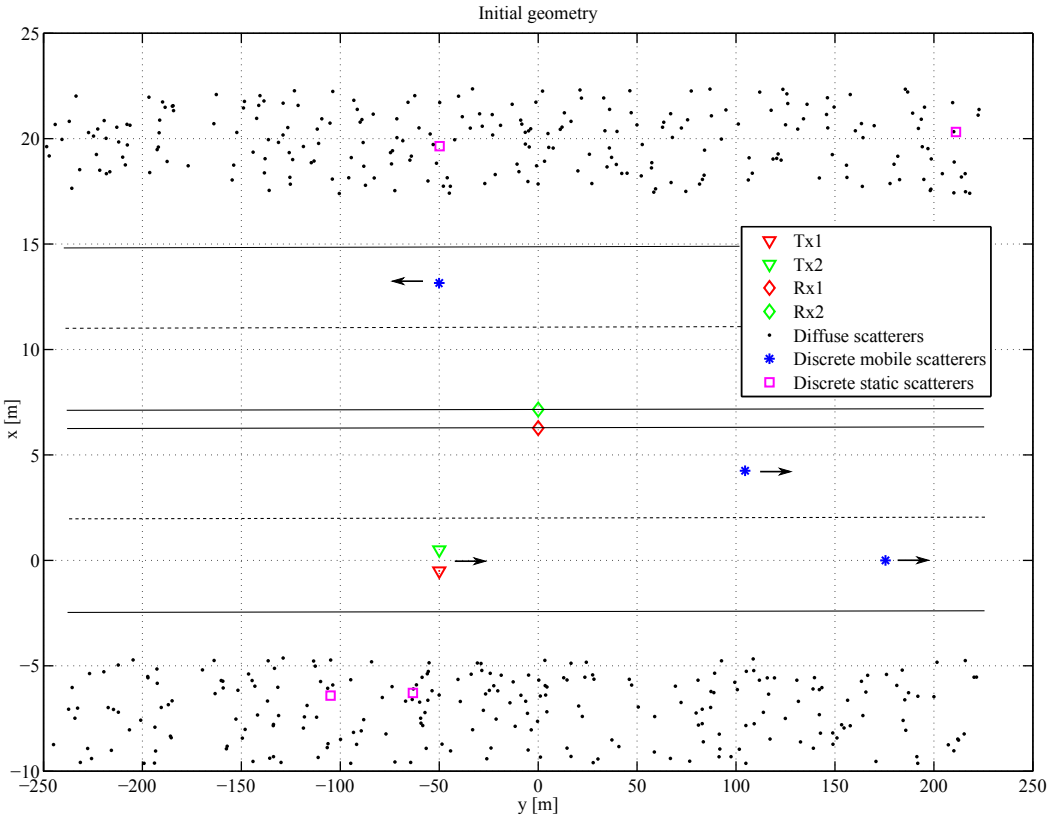

Figure 3.5: Geometry-based Stochastic Channel Model for vehicular highway environment

The position of every distinct transmit and receive antenna as well as the transmitter velocity are input parameters to the model, which allows to analyze various antenna positions and spacing at the vehicle.

The time variant impulse response is modeled by the superposition of various paths as presented in Equation 3.13. The first term considers a single LOS component, which also contains ground reflections, the remaining terms define components originating from mobile discrete (P), static discrete (Q) and diffuse (R) scatterers.

$$h(t,\tau) = h_{LOS}(t,\tau) + \sum_{p=1}^{P} h_{MD}(t,\tau_p) + \sum_{q=1}^{Q} h_{SD}(t,\tau_q) + \sum_{r=1}^{R} h_{DI}(t,\tau_r) \tag{3.13}$$

Nearby cars driving in the same or opposite direction are represented by mobile discrete scatterers whereas road signs are represented by static discrete scatterers. Building structures or foliage along the road belong to diffuse scattering components. The propagation distances concerning each path are varying in time, since the transmitter is moving with a predefined velocity. In contrast to conventional GSCM, this model assumes that the LOS as well as the discrete scatterer contributions are faded. The arrangement of point scatterers expressed in terms of initial position, velocity and occurance density (scatterers per meter) is defined by statistical parameters resulting from real world measurements, as well as the initial gain and path loss component for every considered contribution path. In consequence the speed of mobile discrete scatterers is randomly assigned from a distribution with a mean of 90 km/h and a standard deviation of 2 km/h. Various other parameters like the initial positions of scatterers are derived in a similar manner. For a detailed description of the channel model, the reader is referred to [18]. This GSCM inherently provides the impulse responses for every branch in MIMO transmission, since the computation principle is the same for every link, just the position of the transmit and receive antenna pair differs.

Figure 3.6 depicts a typical GSCM time variant impulse response. In comparison with Jakes spectrum channel model, the channel parameters vary slower. The length of the impulse response is modeled by 30 taps, which differs from Jakes spectrum and the block-fading model. Since the guard interval in IEEE 802.11p consists of 16 taps, a channel impulse response with a duration of 30 taps introduces ISI.

3.2.5 Channel Normalization

Every previously considered virtual channel model requires a normalization process. This is a very important step for simulation issues, since the mean receive and transmit

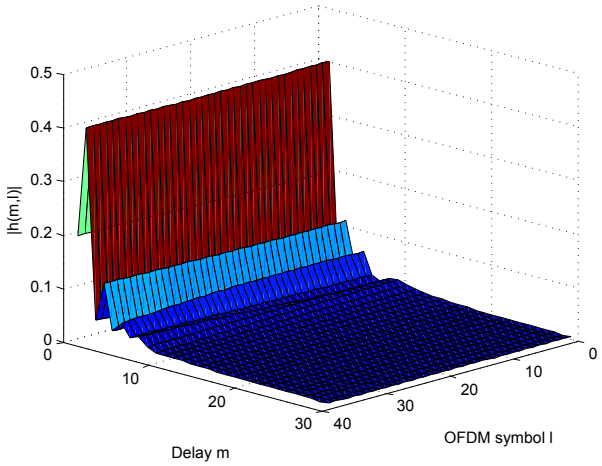

Figure 3.6: Typical GSCM impulse response

power have to be equal in order to obtain valid simulation results. This normalization can be carried out numerically by applying a deterministic factor to every randomly generated impulse response as indicated in Equation 3.14, with N_R representing the number of receive antennas and $||\cdot||_F$ the Frobenius norm. H_n depicts the normalized channel matrix.

$$\mathrm{H}_n = \frac{\sqrt{M_R}}{\sqrt{E\{||H||_F^2\}}}\mathrm{H} \tag{3.14}$$

The channel matrix H comprises the impulse responses for every MIMO branch for one discrete time instant n, as shown in Equation 3.15. The normalization process can be accomplished in the time or in the frequency (subcarrier) domain. These representations are equivalent and related by the discrete Fourier transformation ($h[m] \Longleftrightarrow H[k]$).

$$\mathrm{H} = \begin{pmatrix} h_{1,1}[0] & h_{1,1}[1] & \cdots & h_{1,1}[15] \\ h_{2,1}[0] & h_{2,1}[1] & \cdots & h_{2,1}[15] \\ h_{1,2}[0] & h_{1,2}[1] & \cdots & h_{1,2}[15] \\ h_{2,2}[0] & h_{2,2}[1] & \cdots & h_{2,2}[15] \end{pmatrix} \tag{3.15}$$

For the computation of 3.14 the matrix H must be available to all discrete time instants n during the entire frame duration, or at least the term $E\{||H||_F^2\}$ should be computable. $E\{\cdot\}$ represents the expectation operation over all discrete time instances n.

Neglecting a normalization of the channel will end up in an inappropriate scaling of the channel matrix and distort the simulator outputs in terms of an Eb/N0 shift. This normalization step is carried out in the block-fading and Jakes spectrum channel

model.

3.3 Receiver

Referring to Figure 3.1 the output of the channel model is depicted as the receive signal on each receive antenna in the discrete time domain. The first submodule on the receiver side is the demodulator. One task of the demodulator is to neglect the cyclic prefix. The remaining 64 samples of each OFDM symbol are directed to an FFT block, which converts the data in a time-frequency grid[7]. Equation 3.16 depicts a mathematical representation of the FFT, with k representing the subcarrier index and $N_{FFT} = 64$ as the FFT size.

$$S[k] = \frac{1}{\sqrt{K}} \sum_{n=0}^{K-1} s[n] e^{-j2\pi \frac{nk}{K}}. \tag{3.16}$$

In the case of 2×2 or 2×1 MIMO transmission, the next submodule obtains two or one frame(s) represented in a time frequency grid. Since the simulated transmission consists of the HT-STF, two HT-LTF and the data part, the first OFDM symbol (HT-STF) can be neglected. The symbols containing HT-LTF 1 and HT-LTF 2 are directed to the MIMO channel estimator, where the channel estimation procedure is carried out as defined in Section 2.3.2. It's noteworthy that the channel estimator uses, in total, four symbols to estimate the channel states for two or four channel branches, whereas a pure 802.11p SISO channel estimator uses two symbols to estimate only one channel branch (average LS estimation see [4]). Therefore the MIMO channel estimation procedure results in poorer performance in terms of the channel estimator's MSE. The simulator provides the choice of either using perfect CSI or an LS block based channel estimation obtained from HT-LTF. As depicted in Section 2.2.3 Alamouti STC decoding is implemented with the Least Square equalization procedure utilizing the pseudoinverse of the virtual channel matrix. The implemented decoder for the Golden Code is a Maximum Likelihood Brute Force decoder, as shown in Section 2.2.4. Utilizing space-time codes, there is no conventional equalization procedure as in SISO system. The equalization process is carried out in conjunction with the STC decoding part. The outputs of the Alamouti decoding procedure are soft symbols, whereas the Golden Code ML BF decoder provides hard symbol outputs[8]. Hard-demapping, based on the minimum Euclidean distance from every distinct receive soft symbol to the set

[7] After the FFT a subcarrier rearrangement is carried out, defined in IEEE 802.11p specifications.

[8] Hard symbols are valid symbols of the modulation alphabet ($\hat{a} \in \mathcal{A}$) whereas soft symbols generally are in between hard symbol points in the complex plane.

of transmitted symbols from the alphabet $\mathcal{A}$, is processed by a slicer with a decision rule, provided in Equation 3.17. This decision is carried out in a symbol-per-symbol manner.

$$\hat{a} = \arg \min_{a \in \mathcal{A}} ||r - a|| = \arg \min_{a \in \mathcal{A}} \sqrt{(r_I - a_I)^2 + (r_Q - a_Q)^2}. \tag{3.17}$$

Next, the estimated hard symbol stream is converted into an estimated bit stream by inverting the mapping procedure performed at the transmitter. Thereafter the deinterleaver inverts the rearrangement procedure accomplished by the interleaver. For FEC decoding issues, IEEE recommends a Viterbi algorithm. This algorithm provides a Maximum Likelihood decoding capability for the received bit sequence implemented in an efficient manner. The decoding decision rule is shown in Equation 3.18, with r representing the receive bit sequence and s the transmitted bit sequence.

$$\hat{s} = \max_{s} \Pr(r|s), \tag{3.18}$$

In this way the payload data bits $\hat{s}$ are estimated at the receiver. For BER computation, the estimated decoded data bits are compared with the initial payload data.

Channel State Information for Decoding

Alamouti and the Golden Code transmission schemes assume that the CSI, i.e. the channel gains, do not change during the transmission of two consecutive symbols. In OFDM systems, this assumption indicates that the CSI remains static during two OFDM symbols[9]. Thus, the coherence time (3.7) defined by vehicular channel conditions must be longer than $16\,\mu$s. Vehicular channel measurements provided in [15] state that this assumption holds also in worst case channels, i.e. highway environment. The channel state variation is minimal during two symbols. Therefore, the quality of the transmission should not be decreased considerably by this circumstance.

For 2×2 and 2×1 transmission, the CSI for four or two links is needed at the transmitter for decoding. This information is provided by the impulse responses $h_{i,j}[n, m]$ with the discrete delay m and the discrete time n. The impulse response for an arbitrary link $h[m]$ can be viewed with the dependence of the OFDM symbol index l, depicted by $h[l, m]$. This term can be transformed in a frequency domain by the FFT operation of length $N_{FFT} = 64$, resulting in the channel gain representation $H_{i,j}(k, l)$ with k representing the subcarrier index, as depicted in Figure 3.7.

The transmission of STC codesymbols c obtained from two consecutive symbols x_1

[9] IEEE 802.11p defines an OFDM symbol duration of $8\,\mu$s.

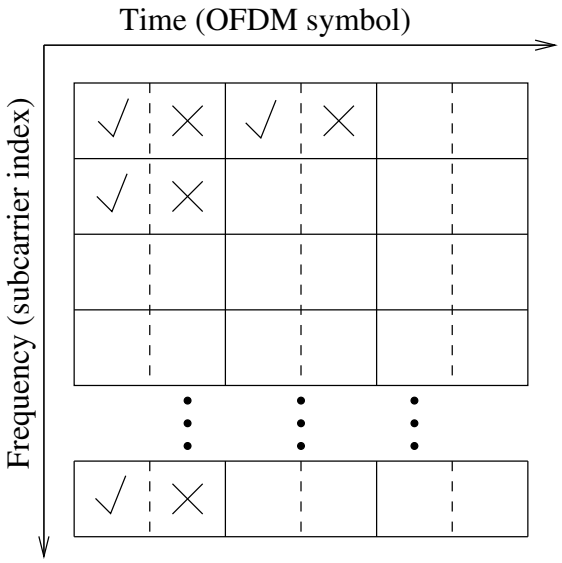

Figure 3.7: Channel State Information

and x_2 is spanned over two OFDM symbols. Generally speaking, the channel gains vary slight during the transmission of two consecutive OFDM symbols. This fact is not taken into account in [6]. Therefore, it is assumed to use the first channel gain (coefficient) and neglecting the second in order to decode.

3.3.1 Eb/N0 Definition

For the comparison of different transmission and detection systems a unitary approach must be considered. A common way of comparing various transmission schemes is to consider how much energy is needed to transmit a single payload bit with a specific reliability. The energy per bit to noise power spectral density ratio E_b/N_0 is a normalized signal to noise power ratio metric.

A compensation factor based on the transmission system depicts how the payload bit energy is spread over the discrete time output signal. This compensation is presented in Equation 3.19. The following properties have to be taken into consideration.

- Bits per subcarrier (bits per symbol)
- FEC code rate
- Preamble size
- Comb pilot subcarriers
- Guard interval

- Space-time code rate

Equation 3.19 depicts how the signal to noise (S/N) power ratio is derived form the simulator input parameter Eb/N0 in a linear form. S/N is used to prescribe the noise power at the receiver. The abbreviations used in this equation are depicted in Table 3.3. This arrangement considers the E_b/N_0 ratio at the transmitter and allows a direct comparison of systems with different modulation and encoding schemes (FEC and STC).

$$\frac{S}{N} = \frac{E_b}{N_0} N_{BPS} C_{FEC} \frac{N_{dataSym}}{N_{dataSym} + N_{preSym}} \frac{N_{dataSub}}{N_{dataSub} + N_{combSub}} \frac{N_{FFT}}{N_{FFT} + N_{guardInt}} C_{STC} \tag{3.19}$$

Abbreviation	Full name	Value range
N_{BPS}	Number of bits per subcarrier	1,2,4
C_{FEC}	Code rate FEC	1/2, 2/3, 3/4
$N_{dataSym}$	Number of data OFDM symbols	dependent on payload size
N_{preSym}	Number of preamble OFDM symbols	8 (3 Non-HT, 5 HT)
$N_{dataSub}$	Number of data subcarriers	48
$N_{combSub}$	Number of comb pilot subcarriers	4
N_{FFT}	FFT size	64
$N_{guardInt}$	Guard interval size	16
C_{STC}	Space-time code rate	Alamouti: 1/2, Golden Code: 1

Table 3.3: Transmission parameters

In order to provide a fair comparison of four transmit schemes, the total transmit energy must be equal for all schemes. In other words, the transmission of one frame utilizes the same energy in SISO, Alamouti and Golden Code. Therefore the mean transmit power in the simulator on each spatial stream is 1, 1/2[10], 1 for SISO, Alamouti and Golden Code, respectively in order to obtain the same transmit energy[11].

3.3.2 Simulator Output

The MIMO simulator provides evaluations of predefined transmission and detection systems. The following list provides an overview of important simulation parameters.

[10]For simulation reasons the mean transmit power of each antenna in Alamouti is 1, but the noise variance is doubled.

[11]Note that the transmit duration of Golden Code is half of SISO and Alamouti.

- Transmitter: Regime, code rate (FEC), modulatin scheme, space-time code, cyclic delay, transmitter velocity
- Channel model: AWGN, block fading (with link correlations), Jakes spectrum time variant model, GSCM
- Receiver: Hard-decision, Zero Forcing or Maximum Likelihood Brute Force decoding for STC, channel estimation (perfect CSI or Least Square block type estimator)

The simulator provides outputs in terms of BER versus E_b/N_0 curves. The uncoded BER (bit stream before Viterbi-decoding) and the BER are visualized. In addition the MSE of the channel estimator, which is the difference between the exact CSI and the estimated CSI of all transmit branches (added up) are provided. Due to the high complexity of the ML BF decoder only the regimes 1-6 depicted in Table 1.2 are implemented for the Golden Code.

4

Simulation Results

This chapter provides the simulation results obtained from the IEEE 802.11p PHY simulator with implemented MIMO transmission schemes. The performance of MIMO schemes is compared with IEEE 802.11p SISO simulation results. For each channel model mentioned in Chapter 3 an evaluation of space-time codes, as introduced in Chapter 2, is provided. Different simulation parameters were investigated in order to evaluate the performance increase promised by MIMO transmission systems. For evaluations presented here we have used transmission regimes 3 and 5, due to their reliability and relevance for vehicular communications. In order to accomplish channel estimation, Least Square block-type channel estimators are used for SISO, as well as for multi-antenna schemes. For decoding the Alamouti schemes we have used a ZF decoder, for the Golden Code a ML BF decoder and for SISO a ZF equalizer.

4.1 AWGN Channel

First evaluations are carried out with a simple AWGN channel model. It assumes neither multipath propagation nor time variance. Although it is not a very realistic model, it helps to analyze key transmission settings. For SISO transmission channel $h[n, m]$ is modeled as a delta impulse $\delta[m]$, constant for every time instance n. MIMO channel properties are depicted in Table 3.2.

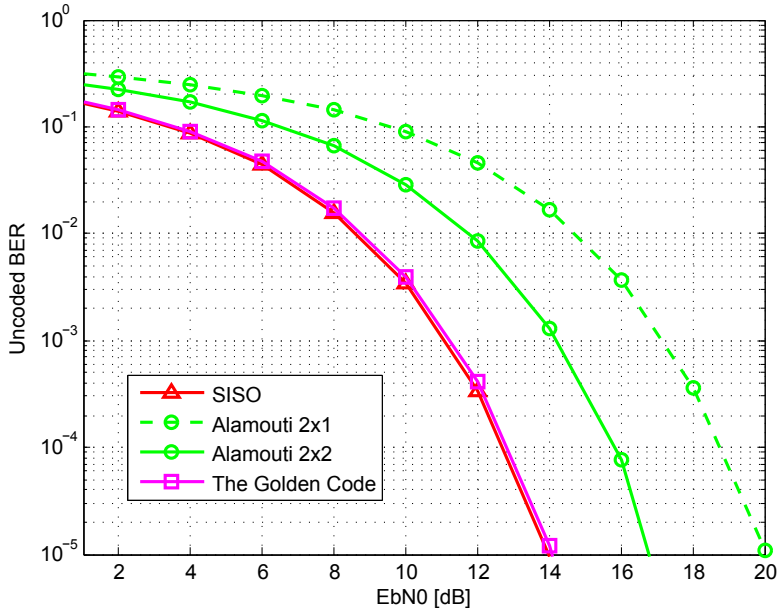

Figure 4.1: AWGN model 1, QPSK, code rate: 1/2, frame length: 2000 bytes, 500 frames, perfect CSI

AWGN Model 1

For 2×2 schemes the AWGN model 1 is considered, whereas for Alamouti 2×1 transmission every link impulse response is represented by a delta impulse. Figures 4.1 and 4.2 show the uncoded BER and BER with perfect CSI for decoding, respectively. The evaluation process is carried out with a frame length of 2000 bytes and 500 frames.

For this channel model, SISO transmission as well as Golden Code 2×2 provide nearly equal performance. The slight shift between SISO and the Golden Code represents the fact, that MIMO schemes apply a longer preamble. Alamouti 2×2 shows an offset of 3 dB compared to the latter mentioned schemes. In an AWGN channel, multi-antenna schemes do not pay off, due to the fact that no fading effects are simulated. Nevertheless, Golden Code provides double data rate with the same reliability as SISO transmission. Common wireless channel effects like multipath fading are neglected by the AWGN channel. The overall diversity order of this channel, which is defined by the slope of the BER curve, is infinity. This holds for MIMO AWGN channels as well, since the utilization of multi-antenna schemes cannot further increase the diversity order.

Next, the evaluation shown in Figures 4.3 and 4.4 provides the BER and the channel estimator's MSE from similar settings as the latter, however with a LS block-type channel estimator, as provided in Section 2.3.2.

Figure 4.3 shows that MIMO schemes need higher transmission power than pure 802.11p SISO transmission in order to obtain the same reliability. The main reason why

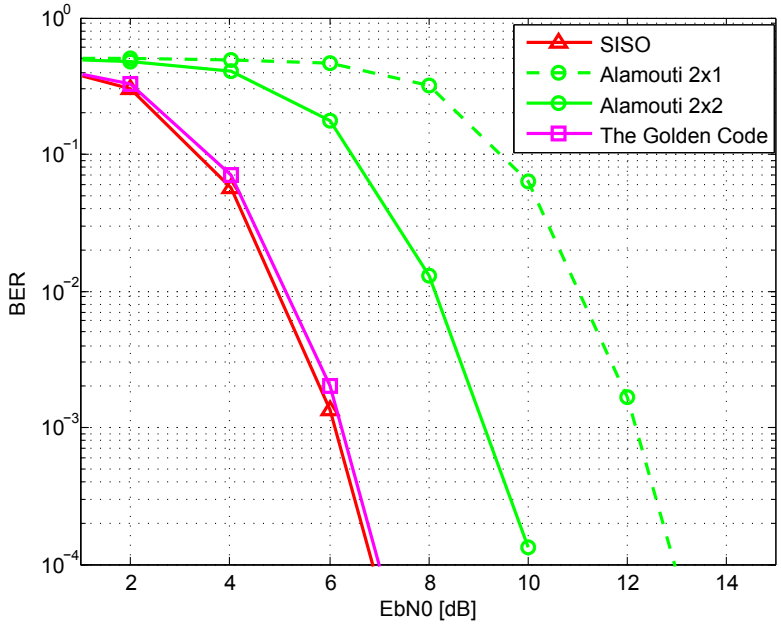

Figure 4.2: AWGN model 1, QPSK, code rate: 1/2, frame length: 2000 bytes, 500 frames, perfect CSI

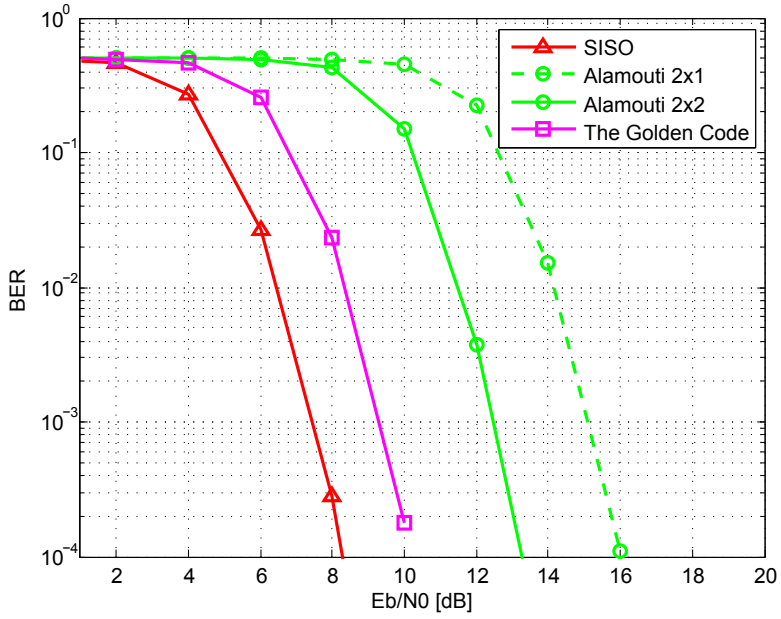

Figure 4.3: AWGN model 1, QPSK, code rate: 1/2, frame length: 2000 bytes, 300 frames, LS block-type channel estimation

MIMO schemes perform worse is that the MIMO LS channel estimator provides higher MSE than the SISO LS channel estimator, as depicted in Figure 4.4. This is related to the fact that SISO utilizes two OFDM preamble symbols to estimate one channel impulse response (averaging LS channel estimator). A MIMO LS channel estimator estimates two or four impulse responses by utilizing two OFDM symbols. Therefore no

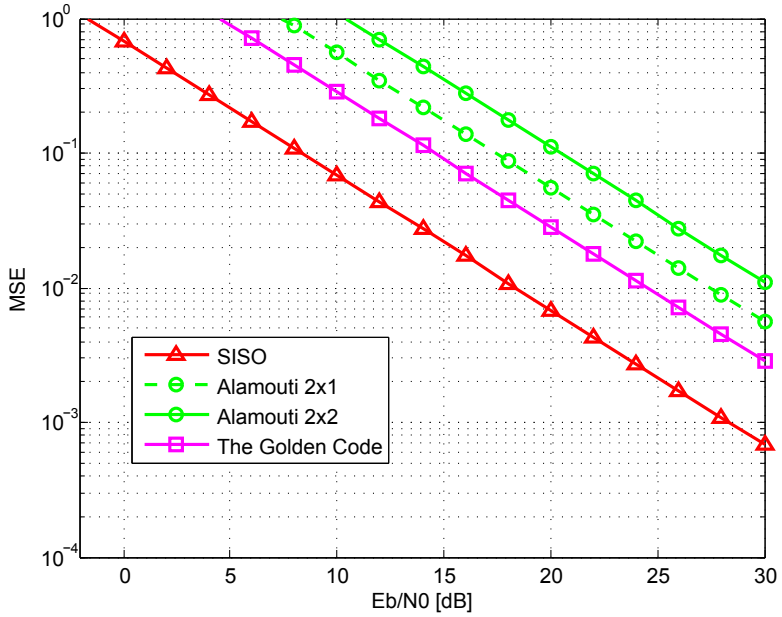

Figure 4.4: AWGN model 1, QPSK, code rate: 1/2, frame length: 2000 bytes, 300 frames, LS block-type channel estimation

averaging process is accomplished, this results in higher MSE.

The estimation principle for Alamouti 2×2 and Golden Code are identical. Nevertheless, a 6 dB shift occurs in Figure 4.4. This shift derives from two distinct properties. First, Alamouti uses half the transmission power compared to Golden Code, this holds also for the transmission of preamble symbols. Therefore, the Golden Code provides a 3 dB lower MSE. The second shift of 3 dB is related to Equation 3.19, due to the utilization of the space-time code rate. These properties are described in Section 3.3.1. The channel estimator of Alamouti 2×1 shows a lower MSE than 2×2, since it has to estimate only two link branches. This statement is also valid in other channel models and must be considered for further MSE plots.

AWGN Model 2

Simulation results for AWGN channel model 2 used for 2×2 transmission schemes are shown in Figure 4.5. The channel matrix described for every subcarrier $\mathrm{H} = \begin{pmatrix} 1 & 1 \\ 1 & 1 \end{pmatrix}$, is a singular matrix and provides a worst case MIMO channel. Alamouti is capable of handling this channel model, whereas the Golden Code shows a considerable performance decrease.

In conclusion, we can say that the pure AWGN already provides a diversity order of infinity. Thus, increasing the diversity by the utilization of multi-antenna systems does not have any effect at all. The insufficient MIMO channel estimator and the increased

preamble length result in a degradation of system performance, since the comparison is accomplished with Eb/N0 metrics.

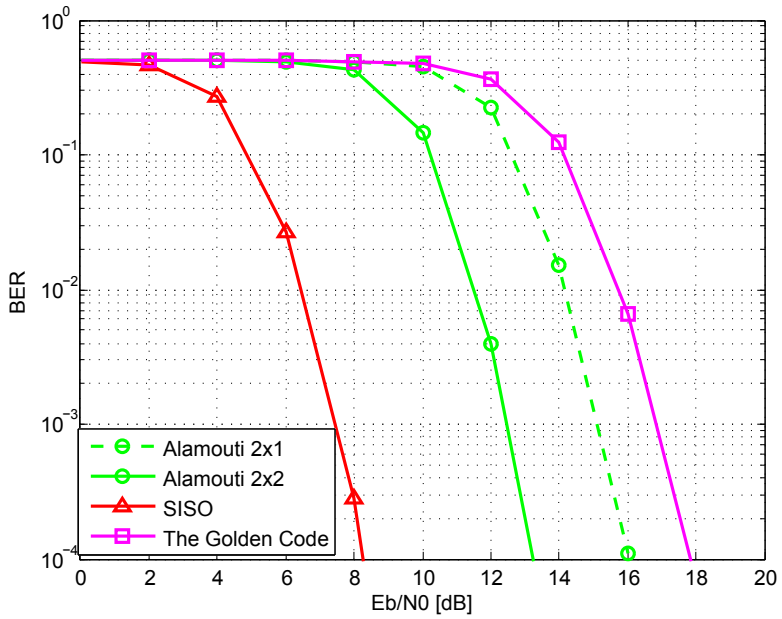

Figure 4.5: AWGN model 2, QPSK, code rate: 1/2, frame length: 2000 bytes, 500 frames, LS block-type channel estimation

4.2 Block-Fading Channel

This section presents the simulation results for the block-type Rayleigh fading channel with exponential decaying PDP, as introduced in Section 3.2.2. In contrast to the pure AWGN channel, this channel model assumes multipath propagation resulting in frequency selective fading. The equalization process (SISO) and the STC decoding process (MIMO) will compensate for frequency selective fading effects introduced by the channel. Due to the fact that the CSI remains constant during the entire frame duration an LS block-type channel estimator is appropriate.

Least Square Channel Estimation

Figure 4.6 depicts evaluations of transmission regime 3. The SISO evaluation applies a Zero Forcing equalizer and an LS channel estimator. All multi-antenna schemes use an LS block-type channel estimator. As mentioned in the previous section, the MIMO LS channel estimator shows higher MSE. This fact degrades the MIMO performance also in block fading channels. As presented in Figure 4.6, the SISO scheme performs better than the multi-antenna schemes for low SNR. Nevertheless, the slope of MIMO schemes

is steeper compared to SISO. Thus, the advantage of Alamouti and Golden Code will pay off at higher SNR. Assuming a BER of 10^{-3} Alamouti 2×2 and the Golden Code provide a reduction of about 1 dB in terms of transmit power requirements. The performances of Alamouti 2×2 and the Golden Code are quite the same. Figure 4.7 reveals the MSE of the channel estimator, which provides similar behavior as in the case of an AWGN channel.

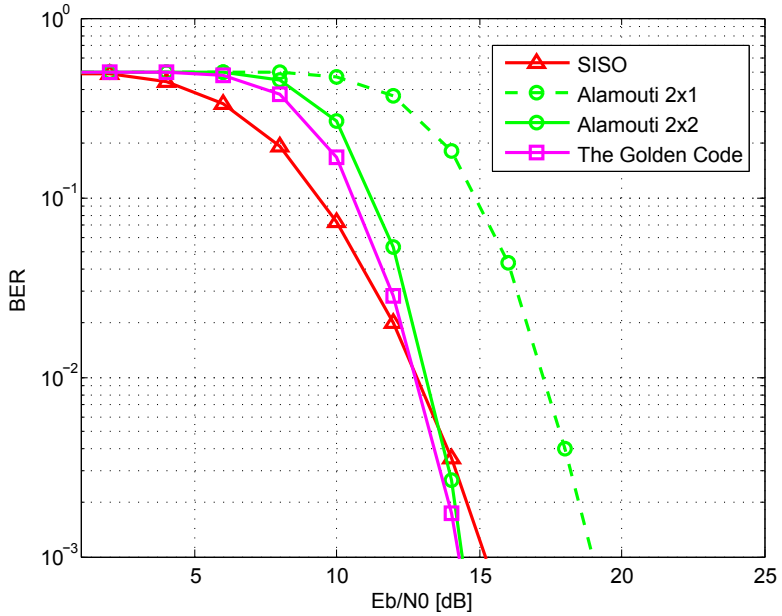

Figure 4.6: Block-fading, QPSK, code rate: 1/2, frame length: 2000 bytes, 500 frames, LS block-type channel estimator

Figure 4.8 shows the evaluation with 16-QAM modulation and a code rate of 1/2. The other simulation parameters remain the same as in previous evaluations.

Perfect CSI

Recalling Figure 4.6, the MIMO channel estimator needs improvement. Therefore, simulations with perfect CSI are presented in Figure 4.9. The results in this figure provide a perspective of how the reliability can be increased by using more sophisticated channel estimators.

Kronecker Model - Correlations

Correlations of various transmission paths will affect the transmission quality in real world environments. These correlations appear in insufficient scattering environments. The implementation of correlated links are defined by the coefficients ρ_{Tx} and ρ_{Rx} introduced by the Kronecker model in Section 3.2.2.

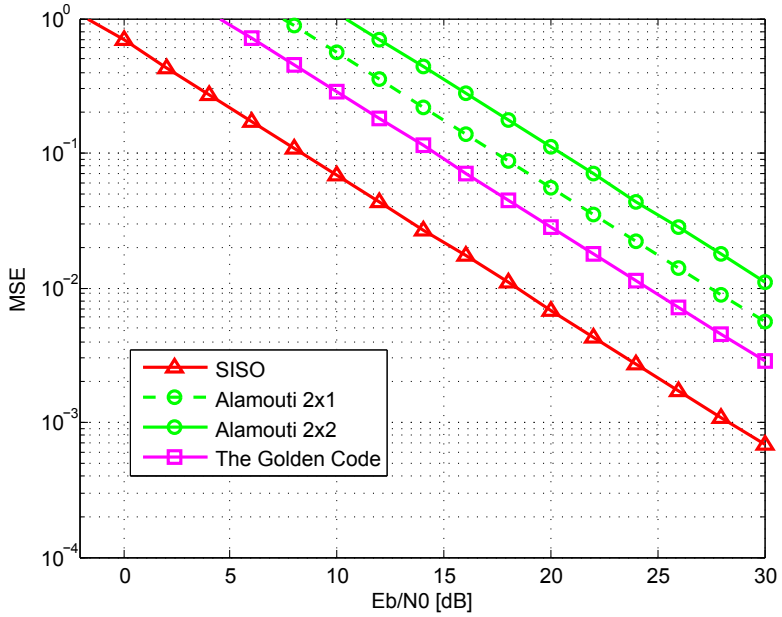

Figure 4.7: Block-fading, QPSK, code rate: 1/2, frame length: 2000 bytes, 500 frames, LS block-type channel estimator

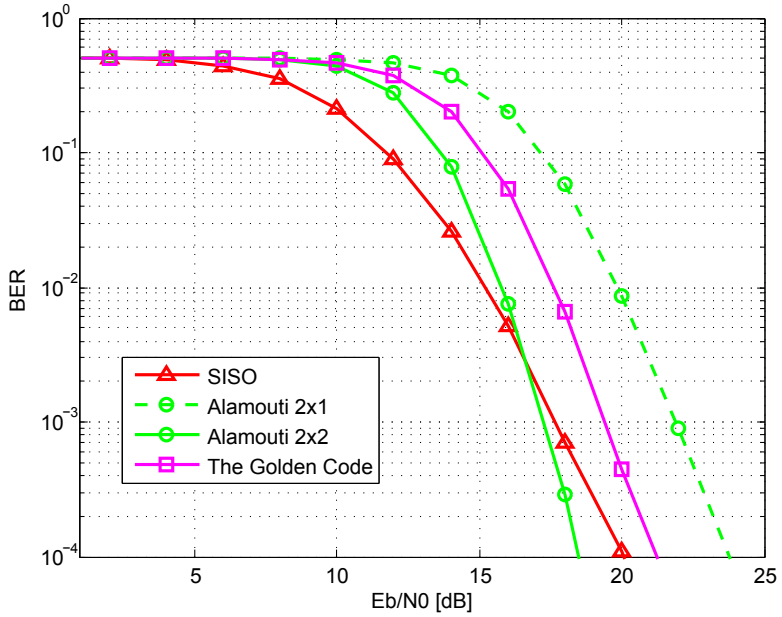

Figure 4.8: Block-fading, 16-QAM, code rate: 1/2, frame length: 2000 bytes, 500 frames, LS block-type channel estimation

Figure 4.10 shows evaluations for Alamouti 2×2 with various correlation coefficients. Transmission reliability suffers significantly by utilizing correlated links. Applying correlations near to 1, the channel instants become the same. Obviously, simulations with $\rho_{Tx} = 0.99$ and $\rho_{Rx} = 0.99$ provide worse transmission quality. If fading occurs, it affects all links in the same manner, therefore all four channel instants are equal. Similar

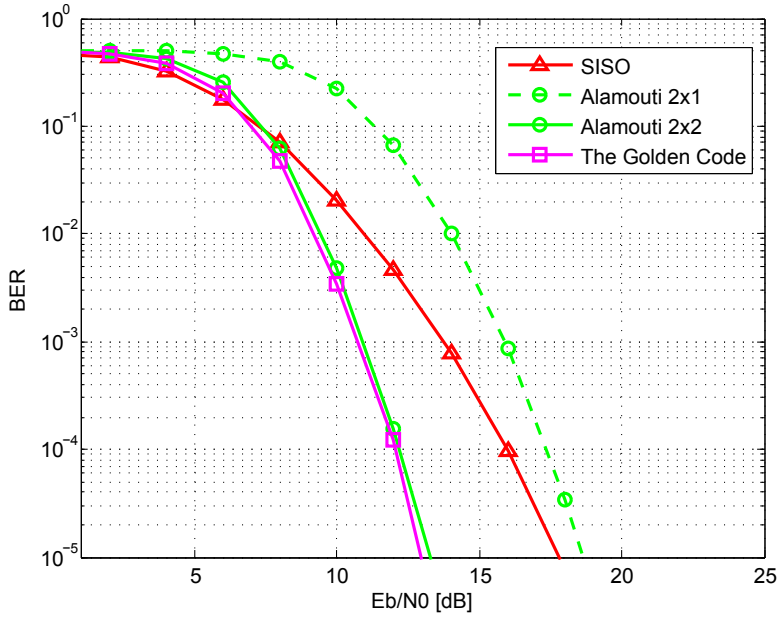

Figure 4.9: Block-fading, QPSK, code rate: 1/2, frame length: 2000 bytes, 500 frames, perfect CSI

evaluations are carried out for the Golden Code in Figure 4.11, which is more sensitive to correlated links.

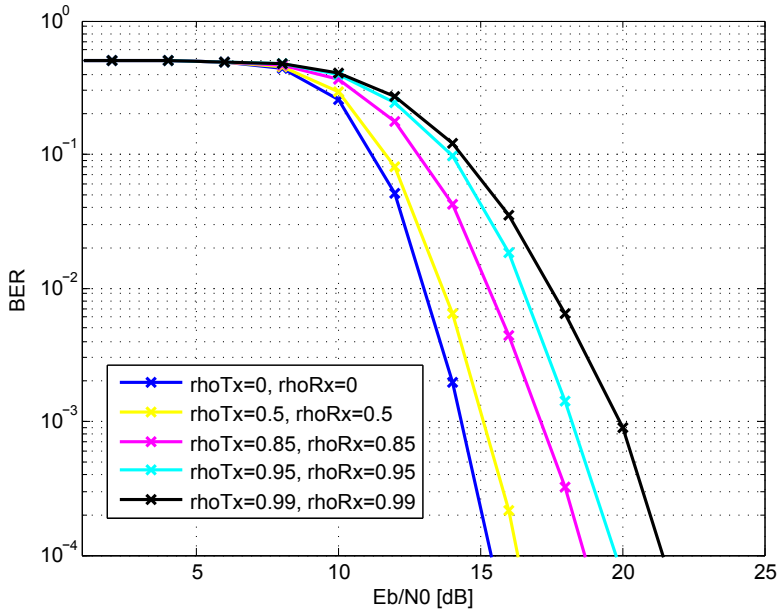

Figure 4.10: Alamouti 2×2, block-fading with Kronecker model, QPSK, code rate: 1/2, frame length: 2000 bytes, 300 frames, LS block-type channel estimation

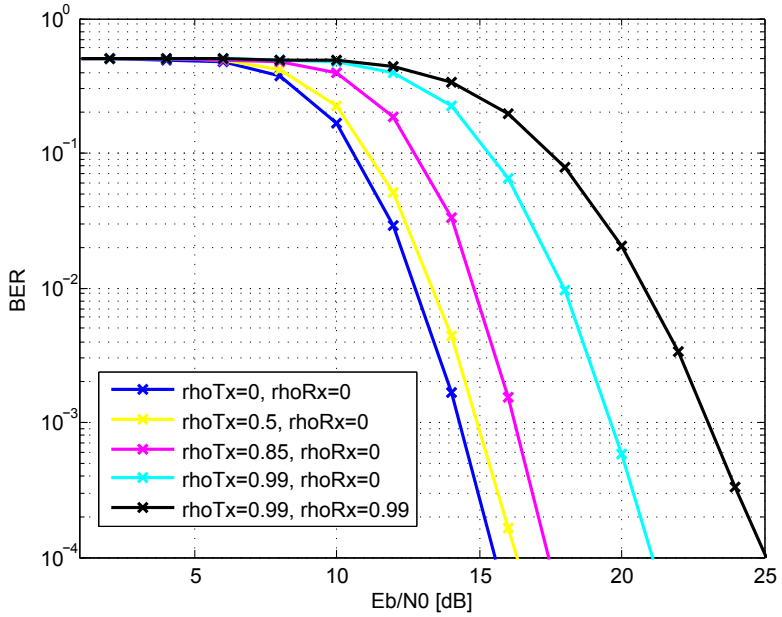

Figure 4.11: Golden Code, block-fading with Kronecker model, QPSK, code rate: 1/2, frame length: 2000 bytes, 300 frames, LS block-type channel estimation

4.3 Jakes Spectrum Channel Model

This time-variant channel model has been introduced in Section 3.2.3. It is capable of modeling fast varying NLOS channel conditions due to a relative movement of transmitter and receiver. All analysis accomplished in this section assume the velocity of 100km/h, in contrast to the previously considered block-fading channel model, in which static channel states are assumed.

Least Square Channel Estimation

Since the channel state changes in this time variant channel model, the estimated CSI is outdated quickly. Thus, simulations with longer frame durations will end up by having higher error rates. The equalizer estimates the symbols with outdated channel coefficients, which leads to an error floor. The degradation of transmission reliability for short frame lengths is less, compared to longer frame lengths.

Figures 4.14 and 4.13 show evaluations with a LS block-type channel estimator, which is obviously not suitable for time variant channels. Nevertheless these evaluations are carried out because they reveal interesting properties. In fact, Alamouti 2×2 reaches the error floor at around 10^{-4}, whereas the Golden Code provides even a lower error floor. We have to take into consideration, that the Golden Code needs only half the transmission duration of the other schemes. Therefore, the utilized channel coefficients are less outdated, resulting in higher reliability. These evaluations are accomplished

with a frame length of 150 bytes. The higher the frame length, the more outdated are the channel coefficients, and the worse is the achieved reliability. An important consequence of these evaluations is that Alamouti 2×2 and Golden Code are more capable of handling outdated or even coarse estimated CSI than SISO schemes, due to receive diversity. Additionally, MIMO techniques are capable of handling NLOS conditions in a more appropriate way than the SISO schemes. They provide a substantial reliability increase. Furthermore, the Golden Code benefits from the less outdated CSI obtained by the block-type channel estimator, due to half transmission duration.

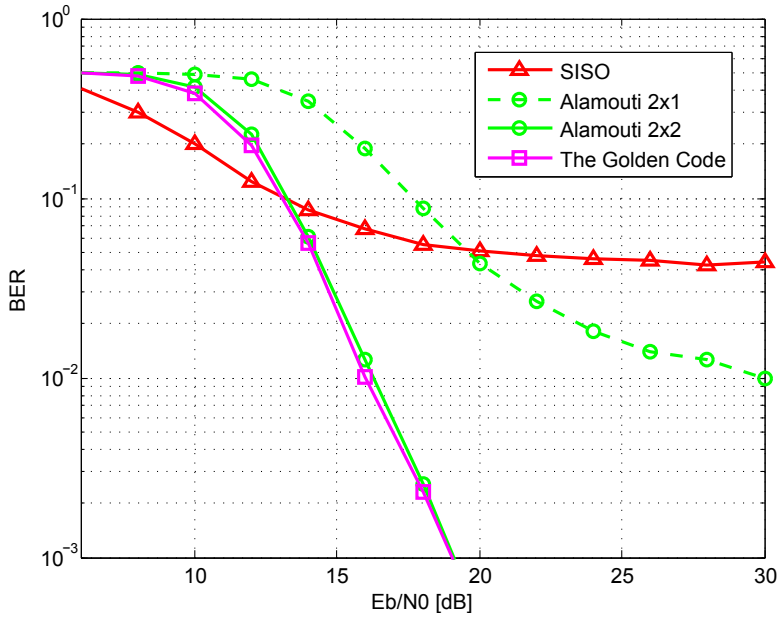

Figure 4.12: Jakes spectrum channel model, QPSK, code rate: 1/2, frame length: 150 bytes, 500 frames, LS block-type channel estimation

Perfect CSI

The results provided in Figure 4.14 show similar performance as in block fading channels depicted in Figure 4.9. Consequently, if the channel states are known, the equalizer or STC decoder is capable of compensating channel effects nearly entirely, also under fast varying channel conditions. The STC decoding procedure assumes that the channel states do not change during the transmission of two consecutive OFDM symbols. The slight CSI change during two symbol durations is neglectable, also in this fast varying channel model.

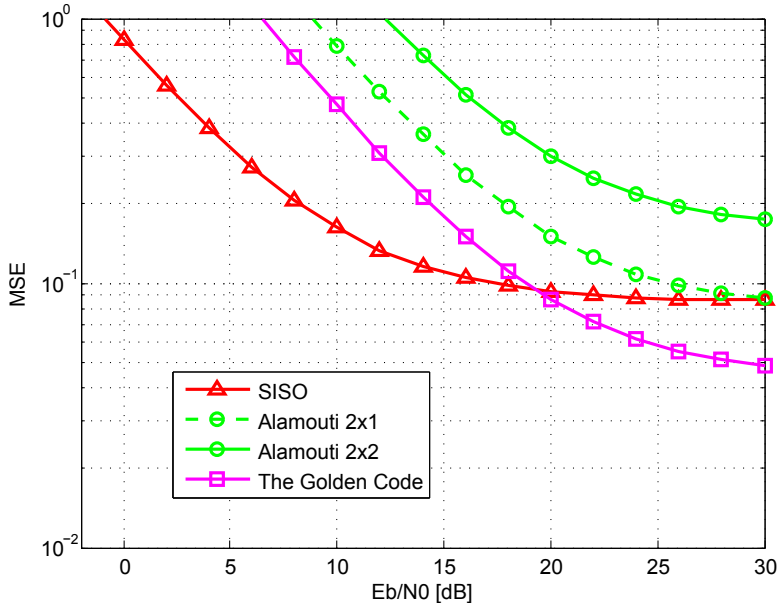

Figure 4.13: Jakes spectrum channel model, QPSK, code rate: 1/2, frame length: 150 bytes, 500 frames, LS block-type channel estimation

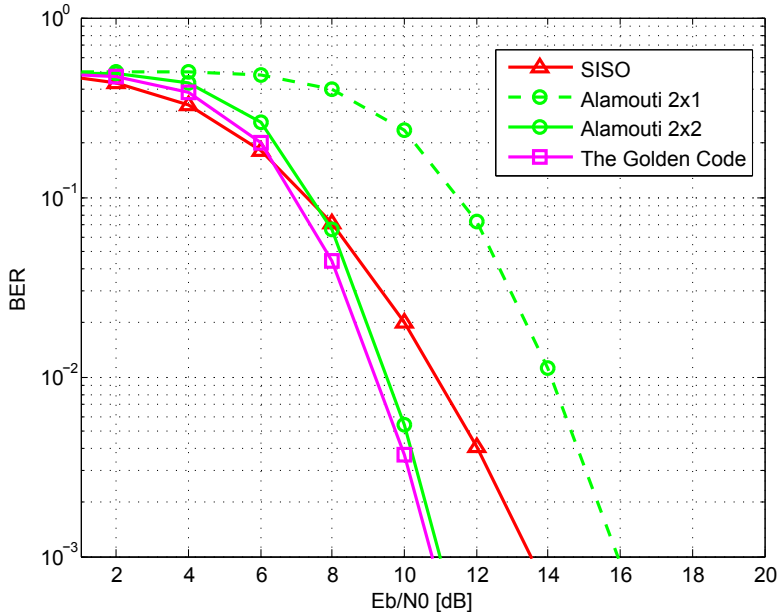

Figure 4.14: Jakes spectrum channel model, QPSK, code rate: 1/2, frame length: 150 bytes, 500 frames, perfect CSI

4.4 Geometry-Based Stochastic Channel Model

This section provides evaluations with the GSCM, introduced in Section 3.2.4. It considers a typical LOS, V2I, highway environment with a moving transmitter and a static receiver. The transmitter car speed is set to 100 km/h in all evaluations. High correlations of channel links decrease the link performance, as shown in Section 4.2. These

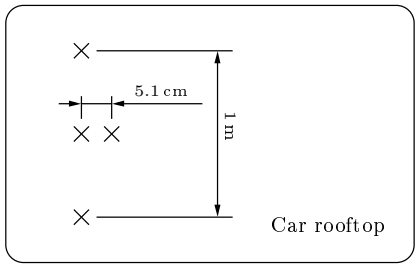

Figure 4.15: GSCM, model 1 and 2 schematic depiction, transmit vehicle

correlations appear in low scattering environment or close antenna spacing. In order to evaluate different transmit antenna spacing distances and thereby possibly occurring correlations, two channel models with different antenna positions are presented in Table 4.1 together with Figure 4.15. The coordinates in the latter mentioned table refer to the coordinate system depicted in Figure 3.5. The two models represent realistic mounting positions on the car rooftop. Model 1 considers a distance of 1 m between the two transmit antennas in x-direction. Therefore two separate antenna modules must be mounted at the vehicle. In order to deploy both WAVE transmit antennas together with other antennas like GPS, 3G/4G in one antenna module, the antenna spacing distance must be decreased. Therefore a distance of $\lambda \approx 5.1\,\text{cm}$ is adopted in y-direction in channel model 2. In all evaluations omni-directional antennas at the transmitter and receiver are implemented. The distance between the receive antennas is set to 1 m, since there is enough space for antenna installation at the gantry. For evaluations of 2×1 and 1×1 systems, transmitter one and receiver one are used (see Table 4.1).

It is noteworthy that in this channel model a double size channel impulse response (30 taps $\hat{=}$ 3 μs) is implemented comparing to previously considered channel models, thereby ISI is introduced.

Model	Pos. Tx 1	Pos. Tx 2	Tx spacing	Pos. Rx 1	Pos. Rx 2	Rx spacing
1	-50/-0.5	-50/0.5	1 m	0/6	0/7	1 m
2	-50.051/0	-50/0	5.1 cm	0/6	0/7	1 m

Table 4.1: GSCM positions (x/y) for model 1 and 2, unit: m

Channel model 1

Perfect CSI

This first channel model determines a separation between transmit of 1 meter. Evaluations are carried out with perfect CSI. Figure 4.16 shows the BER for QPSK transmis-

sion with a code rate of 1/2. The reliability gain achievable by utilizing MIMO schemes in this channel model is less compared to Jakes spectrum or block-fading channel model. This decrease is is due to the fact that the GSCM considers a strong LOS component and less time-variance compared to Jakes spectrum channel model. Although there is a strong LOS component in each link, Alamouti 2×2 provides a substantial reliability and diversity improvement. Utilizing Alamouit 2×1 does not pay off in this channel model, since channel characteristics are similar to the AWGN model 2 (Section 4.1).

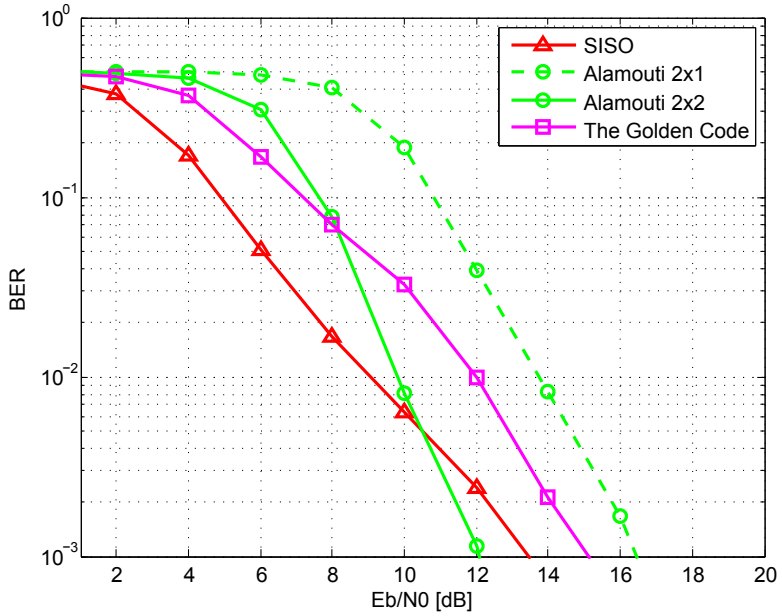

Figure 4.16: GSCM model 1, QPSK, code rate: 1/2, frame length: 200 bytes, 1000 frames, perfect CSI

Least Square Channel Estimator

Evaluations with an LS block-type channel estimator are depicted in Figures 4.17 and 4.18. Due to the time-variance of the CSI, an error floor occurs. Similar to Jakes spectrum channel model, Alamouti 2×2 and Golden Code are capable of handling outdated CSI better due to receive diversity. Figure 4.18 shows the channel estimator's MSE. As described in previous chapters, the MIMO MSE is higher due to a more sophisticated SISO channel estimation procedure.

Channel model 2

The second channel model considers more closely spaced transmit antennas (5.1 cm), in order to place both transmit antennas in one module at the vehicle rooftop. The

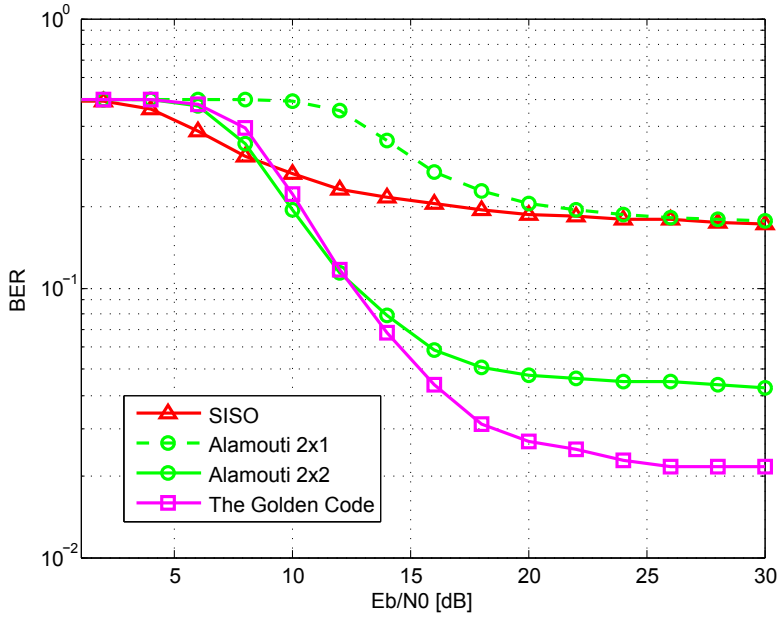

Figure 4.17: GSCM model 1, QPSK, code rate: 1/2, frame length: 200 bytes, 100 frames, LS block-type channel estimation

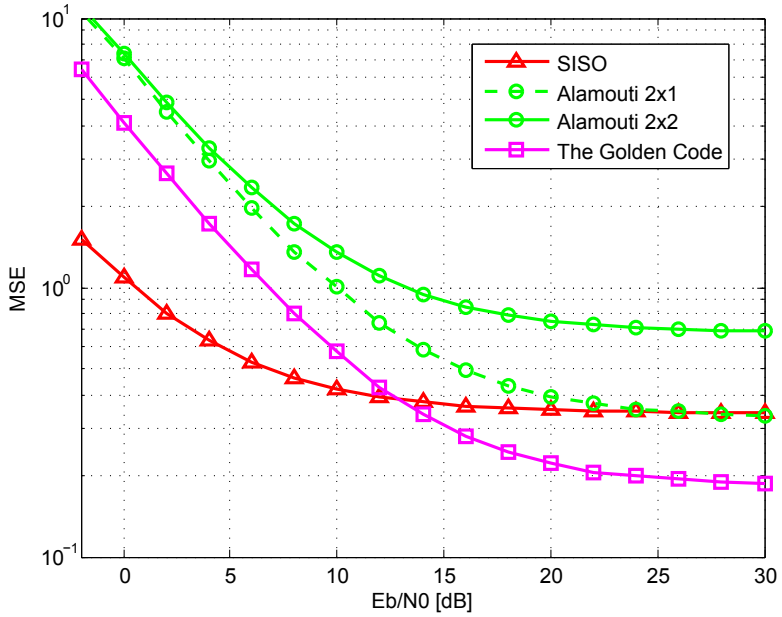

Figure 4.18: GSCM model 1, QPSK, code rate: 1/2, frame length: 200 bytes, 100 frames, LS block-type channel estimation

comparison of Figure 4.16 and Figure 4.19 leads to several significant statements. Reducing the antenna distance to 5.1 cm results in correlated links. Alamouti is capable of handling these correlations and shows a reliability decrease of only 1 dB at a BER of 10^{-3}, whereas the Golden Code is more sensitive to correlated links, as already shown in Section 4.2.

Summarizing the evaluations of simulations with GSCM, we state that in order to obtain higher diversity and reliability one should use larger transmit antenna separation.

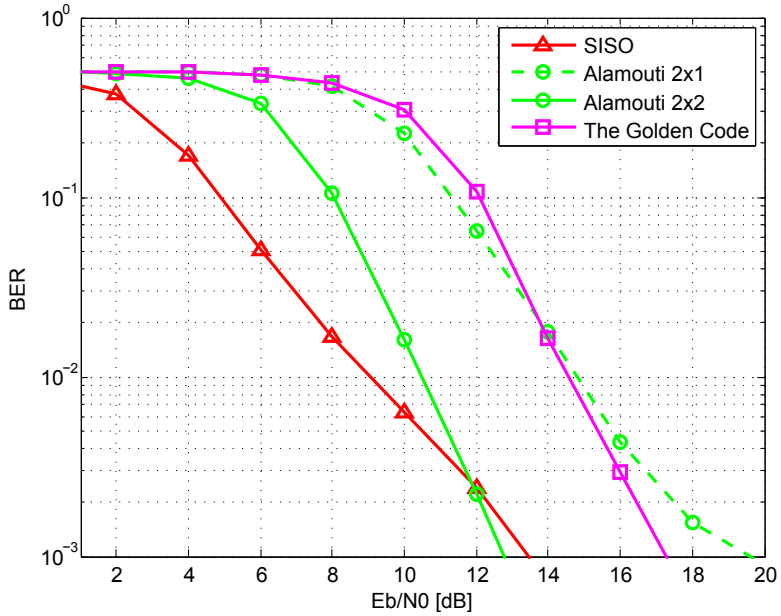

Figure 4.19: GSCM model 2, QPSK, code rate: 1/2, frame length: 200 bytes, 1000 frames, perfect CSI

5

Conclusions

This thesis investigates advantages of utilizing multiple transmit and receive antennas for vehicular communications. It is proposed to use IEEE 802.11n frame structure in order to apply space-time codes, perform MIMO channel estimation and avoid unintentional beamforming effects which would occur when using pure IEEE 802.11p structure. In order to provide statements concerning the deployment, a MIMO WAVE PHY simulator is developed and described. Simulation results present main aspects of space-time codes applied in vehicular communications.

- MIMO transmission schemes provide a significant reliability improvement especially in NLOS environments. Due to the utilization of space-time codes transmission reliability and throughput can be increased.
- The pilot pattern for channel estimation defined by IEEE 802.11n is not optimal for vehicular communications. A significant improvement in terms of MSE can be achieved by utilizing more training data or more sophisticated channel estimators.
- Although the utilized MIMO channel estimation procedure has high MSE, the system performance with Alamouti and Golden Code STBC is not degraded. Due to receive diversity, MIMO schemes are more capable of handling coarse estimated or even outdated CSI than the SISO systems.
- Small antenna correlations do not decrease the performance considerably. Furthermore, the Golden Code is more sensitive to correlated links than Alamouti STC.

- The Alamouti 2×2 transmission scheme is a promising candidate for a multi-antenna system in vehicular communications, since it provides reliable performance for NLOS and LOS radio propagation and low complexity detection schemes.

List of Acronyms

AWGN Additive White Gaussian Noise

BER Bit Error Rate

BF Brute Force

BPSK Binary Phase Shift Keying

CDD Cyclic Delay Diversity

CSI Channel State Information

DS Delay Spread

DSL Delay Spread Length

FEC Forward Error Correction Coding

FFT Fast Fourier Transformation

FTW Forschungszentrum Telekommunikation Wien

GSCM Geometry-based Stochastic Channel Model

IEEE Institute of Electrical and Electronics Engineers

IFFT Inverse Fast Fourier Transformation

ISI Inter Symbol Interference

ITS Intelligent Transport Systems

LAN Local Area Network

LOS Line-of-Sight

LS Least Square

MAC Medium Access Control

MISO Multiple-Input Single-Output

MIMO Multiple-Input Multiple-Output

ML Maximum Likelihood

MMSE Minimum Mean Squared Error

MRRC Maximum Ratio Receiver Combining

MSE Mean Square Error

NLOS Non-Line-of-Sight

OFDM Orthogonal Frequency Division Multiplexing

PDP Power-Delay Profile

PAPR Peak-to-Average Power Ratio

PEP Pairwise Error Probability

PHY Physical Layer

PLCP Physical Layer Convergence Protocol

PMD Physical Medium Dependent

PSDU PLCP Service Data Unit

QAM Quadrature Amplitude Modulation

QPSK Quadrature Phase Shift Keying

RMSDS Root Mean Square Delay Spread

RSU Road Side Unit

SD Sphere Decoder

STC Space-Time Coding

SIMO Single-Input Multiple-Output

SNR Signal-to-Noise-Ratio

V2I Vehicle-to-Infrastructure

V2V Vehicle-to-Vehicle

WAVE Wireless Access in Vehicular Environments

ZF Zero-Forcing

Bibliography

[1] Information Society Technologies, "D.31 European ITS Communication Architecture, Overall Framework, Proof of Concept Implementation." http://www.comesafety.org/uploads/media/, 2008.

[2] IEEE Computer Society, "IEEE standard for information technology - telecommunications and information exchange between systems - local and metropolitan area networks - specific requirements part 11: Wireless LAN medium access control and physical layer specifications." IEEE Std 802.11, June 2007.

[3] IEEE Computer Society, "IEEE standard for information technology–telecommunications and information exchange between systems–local and metropolitan area networks–specific requirements part 11: Wireless LAN medium access control (MAC) and physical layer (PHY) specifications amendment 6: Wireless access in vehicular environments," IEEE Std 802.11p-2010 (Amendment to IEEE Std 802.11-2007 as amended by IEEE Std 802.11k-2008, IEEE Std 802.11r-2008, IEEE Std 802.11y-2008, IEEE Std 802.11n-2009, and IEEE Std 802.11w-2009), pp. 1–51, July 2010.

[4] V. Shivaldova, "Implementation of IEEE 802.11p physical layer model in SIMULINK," Master's thesis, E389, Vienna University of Technology, 2010.

[5] G. Matz and C. Mecklenbräuker, "MIMO communications." Lecture Notes, 2011.

[6] S. M. Alamouti, "A simple transmit diversity technique for wireless communications," IEEE journal on select areas in communications, vol. 16, no. 8, pp. 1451–1458, 1998.

[7] J.-C. Belfiore, G. Rekaya, and E. Viterbo, "The golden code: a 2 x 2 full-rate space-time code with non-vanishing determinants," in Information Theory, 2004. ISIT 2004. Proceedings. International Symposium on, p. 310, July 2004.

[8] S. Yang, J.-C. Belfiore, G. Rekaya, and B. Othman, "Perfect space-time block codes for parallel mimo channels," in Information Theory, 2006 IEEE International Symposium on, pp. 1949 –1953, July 2006.

[9] H. Yao and G. Wornell, "Achieving the full MIMO diversity-multiplexing frontier with rotation-based space-time codes," in PROCEEDINGS OF THE ANNUAL ALLERTON CONFERENCE ON COMMUNICATION CONTROL AND COMPUTING, vol. 41, pp. 400–409, The University, 2003.

[10] "Space-time block codes." http://spacetimecodes.blogspot.com/p/golden-code.html.

[11] M. Sinnokrot and J. Barry, "Fast Maximum-Likelihood decoding of the Golden Code," Wireless Communications, IEEE Transactions on, vol. 9, pp. 26 –31, Jan. 2010.

[12] IEEE Computer Society, "IEEE standard for information technology - telecommunications and information exchange between systems - local and metropolitan area networks - specific requirements part 11: Wireless LAN medium access control and physical layer specifications amendment 5: Enhancements for higher throughput." IEEE Std 802.11n, Oct. 2009.

[13] A. Dammann, S. Plass, and S. Sand, "Cyclic Delay Diversity - A Simple, Flexible and Effective Multi-Antenna Technology for OFDM," in Spread Spectrum Techniques and Applications, 2008. ISSSTA '08. IEEE 10th International Symposium on, pp. 550 –554, Aug. 2008.

[14] R. Van Nee, V. Jones, G. Awater, A. Van Zelst, J. Gardner, and G. Steele, "The 802.11n MIMO-OFDM Standard for Wireless LAN and Beyond," Wireless Personal Communications, vol. 37, pp. 445–453, 2006. 10.1007/s11277-006-9073-2.

[15] C. Mecklenbräuker, A. F. Molisch, J. Karedal, F. Tufvesson, A. Paier, L. Bernadó, T. Zemen, O. Klemp, and N. Czink, "Vehicular channel characterization and its implications for wireless system design and performance," Proceedings of the IEEE, vol. Special Issue on Vehicular Communications, no. 7, pp. 1189–1212, 2011.

[16] A. F. Molisch, Wireless Communications. Chichester (UK): Wiley, 2005.

[17] T. Zemen and C. Mecklenbräuker, "Time-variant channel estimation using discrete prolate spheroidal sequences," Signal Processing, IEEE Transactions on, vol. 53, no. 9, pp. 3597–3607, 2005.

[18] J. Karedal, F. Tufvesson, N. Czink, A. Paier, C. Dumard, T. Zemen, C. Mecklenbräuker, and A. Molisch, "A geometry-based stochastic MIMO model for vehicle-to-vehicle communications," Wireless Communications, IEEE Transactions on, vol. 8, pp. 3646 –3657, July 2009.